Fine chromatin-driven mechanism of transcription interference by antisense noncoding transcription

Authors/Affiliations

Jatinder Kaur Gill[1], Andrea Maffioletti[1], Varinia García-Molinero[1,2], Françoise Stutz[1]* and Julien Soudet[1,3]*.

[1] Dept. of Cell Biology, University of Geneva, 1211 Geneva 4, Switzerland;

[2] Present address: Institut de Génétique Humaine, CNRS - Université de Montpellier, Montpellier, France;

[3] Lead Contact

Contact Info

*Correspondence: julien.soudet@unige.ch (J.S.), francoise.stutz@unige.ch (F.S.)

Summary

Eukaryotic genomes are almost entirely scanned by RNA polymerase II (RNAPII). Consequently, the transcription of long noncoding RNAs (lncRNAs) often overlaps with coding gene promoters triggering potential gene repression through a poorly characterized mechanism of transcription interference. In this study, we propose a global model of chromatin-based transcription interference in *Saccharomyces cerevisiae* (*S. cerevisiae*). By using a noncoding transcription inducible strain, we analyzed the relationship between antisense elongation and coding sense repression, nucleosome occupancy and transcription-associated histone modifications using near-base pair resolution techniques. We show that antisense noncoding transcription leads to -1/+1 nucleosome H3K18/H4 deacetylation associated with H3K36 trimethylation increase (H3K36me3). This results in the loss of -1/+1 nucleosome interaction with the RSC chromatin remodeler and subsequent sliding into the Nucleosome-Depleted Region (NDR) hindering Pre-Initiation Complex (PIC) binding. Finally, we extend our model by showing that natural antisense noncoding transcription significantly represses around 20% of *S. cerevisiae* genes through this chromatin-based transcription interference mechanism.

Keywords

Noncoding transcription, Antisense, Nucleosomes, Histone modifications, Nucleosome-depleted regions, Chromatin remodeler, RSC, Nucleosome resolution, Yeast.

Highlights

-Induction of antisense noncoding transcription leads to -1/+1 nucleosome sliding that competes with sense transcription PIC deposition.

- H3K36me3- and H3K18ac-/H4ac-containing nucleosomes are differently positioned.

- RSC recruitment to -1/+1 nucleosomes is modulated by histone acetylation levels.

- 20% of *S. cerevisiae* genes are significantly repressed by this antisense-dependent chromatin-based transcription interference mechanism.

Introduction

Recent techniques monitoring eukaryotic nascent transcription have revealed that the RNAPII landscape extends far beyond the sole transcription of mRNA (Churchman and Weissman, 2011; Core et al., 2008; Mayer et al., 2015; Nojima et al., 2015). If 1-2% of the human genome is devoted to coding genes, more than 80% is transcribed into >200nt long noncoding RNAs (Djebali et al., 2012). Thus, around 200,000 lncRNAs originating from Nucleosome-Depleted Regions (NDRs) have been recently annotated across different human tissues and cell types (Kaikkonen and Adelman, 2018). While their function is still under debate, it raises a new concept in which RNAPII scans nearly the whole genome as closely interleaved transcription units (Mellor et al., 2016). Consequently, transcription of many lncRNAs is reaching coding gene promoters, eventually leading to transcription interference, *i.e.* repression of the coding gene (Proudfoot, 1986). So far, the precise molecular basis underlying transcription interference remains poorly characterized.

In *Saccharomyces cerevisiae*, noncoding transcription often originates from a NDR, also referred to as bidirectional promoters, transcribing a coding gene in one orientation and a noncoding RNA in the other (Churchman and Weissman, 2011; Jensen et al., 2013; Neil et al., 2009; Xu et al., 2009). Because the yeast genome is compact, a majority of lncRNAs appear as being antisense to coding genes. To avoid antisense transcription into sense paired promoters and to limit transcription interference, lncRNAs are usually subjected to early termination in a process dependent on the Nrd1-Nab3-Sen1 complex followed by degradation (Porrua and Libri, 2015). Early termination of noncoding transcription is not strict and mostly depends on the number of Nrd1-Nab3 recognition motifs carried by the lncRNA (Castelnuovo et al., 2014; Schulz et al., 2013). This implies that some long noncoding RNAs will be cleared through early-termination while others will naturally extend into sense promoters, followed by export and degradation in the cytoplasm *via* Nonsense-Mediated Decay (NMD) (Malabat et al., 2015; van Dijk et al., 2011; Wery et al., 2018). Importantly, artificial loss of early termination through Nrd1 depletion leads to antisense elongation into paired sense promoters and to a subsequent transcription interference directly correlated with the levels of lncRNA accumulation over the promoters (Schulz et al., 2013). According to this view, high steady state levels of natural antisense transcription into gene promoters may anticorrelate with coding sense expression. However, this question is still open since some analyses have led to opposite conclusions (Brown et al., 2018; Murray et al., 2015; Nevers et al., 2018).

RNAPII transcription has an impact on chromatin structure (Rando and Winston, 2012; Venkatesh and Workman, 2015; Zentner and Henikoff, 2013). First, the mean spacing between nucleosomes correlates with transcription frequency (Chereji et al., 2018). The more a gene is transcribed, the more the distance between nucleosomes decreases. Second, RNAPII elongation is associated with concomitant deposition of histone modifications. The Carboxy Terminal Domain (CTD) of RNAPII interacts with Histone Methyl Transferases (HMT) catalyzing the transfer of methyl groups to histone H3. Among them, trimethylation of H3 at lysine 36 (H3K36me3) by Set2 follows a specific pattern over coding genes, being enriched at mid- to end of genes. This modification is a recruitment platform for the Rpd3S Histone DeACetylase (HDAC) complex which can deacetylate H3 and H4 histones (Carrozza et al., 2005; Keogh et al., 2005; Rundlett et al., 1996). Accordingly, H3 and H4 acetylations anticorrelate with H3K36me3, being more enriched at -1 and +1 nucleosomes flanking the promoter NDRs (Sadeh et al., 2016; Weiner et al., 2015). Deletion of *SET2* or *RPD3* leads to intragenic cryptic transcription associated with an increase of histone acetylation along gene bodies (Carrozza et al., 2005; Joshi and Struhl, 2005; Kim et al., 2016; Li et al., 2003; Malabat et al., 2015; Venkatesh et al., 2012; Venkatesh and Workman, 2015). Thus, transcription-associated methylation of nucleosomes and subsequent deacetylation can be considered as a locking mechanism - limiting spurious transcription initiation events.

Interestingly, noncoding transcription-mediated transcription interference usually requires RNAPII-dependent nucleosome modifications. Indeed, loss of Set2 or HDACs leads to a rescue of coding gene expression when noncoding transcription elongates into promoter NDRs (Camblong et al., 2007; Castelnuovo et al., 2014; du Mee et al., 2018; Kim et al., 2016; Nevers et al., 2018; van Werven et al., 2012). Moreover, the more nascent transcription enters into sense promoters at steady-state, the more the NDR becomes narrow (Dai and Dai, 2012; Murray et al., 2015). Altogether, these data suggest that antisense-mediated transcription interference probably occurs through a nucleosome-based mechanism. Indeed, nucleosome positioning at NDRs is crucial for the accessibility of the transcription Pre-Initiation Complex (PIC) to promoters, mainly through the recruitment of the TATA-Binding Protein (TBP, Spt15 in *S. cerevisiae*) at TATA (or TATA-like) Binding Sites (TBSs) (Kubik et al., 2018; Rhee and Pugh, 2012). Importantly, genome-wide NDR opening and subsequent ability to recruit the PIC mainly depends on the RSC ATP-dependent chromatin remodeler (Badis et al., 2008; Hartley and Madhani, 2009; Klein-Brill et al., 2019; Kubik et al., 2018).

In this study, we aim at defining a comprehensive mechanism of antisense-mediated transcription interference through a variety of genome-wide approaches. We use a strategy in

which antisense noncoding early termination can be turned off, leading to inducible transcription interference of more than 200 genes. Systematic analyzes of transcription initiation, NDR chromatin structure and transcription-associated histone modifications reveal the choreography of chromatin-related events associated with lncRNA-induced transcription interference. We then validate our model by defining to which extent the *S. cerevisiae* genome is influenced by this chromatin-based transcription interference at steady state.

Results

Induction of antisense noncoding transcription into paired sense promoters decreases PIC binding

To investigate the mechanism of transcription interference by antisense noncoding transcription, we first defined the list of coding genes that are repressed upon abrogation of RNAPII early termination. To do so, we performed RNA-seq of the Nrd1-Anchor Away (AA) strain in which Nrd1 can be artificially depleted from the nucleus upon Rapamycin (Rap) addition (Figure 1A) (Haruki et al., 2008; Schulz et al., 2013). We then classified the genes into three categories, i) the Antisense-Mediated Repressed Genes (AMRG, 217 genes), showing at least 2-fold increase in antisense and >20% sense repression, ii) the Non-Responsive Genes (NRG, 469 genes), with a minimum 2-fold increase in antisense but less than 20% decrease in sense expression and, iii) the Other Genes (4089 genes), showing less than 2-fold increase in antisense (Figures 1A and 1B). Taking these 3 groups, we observe a prominent correlation between the fold-increase of antisense levels over the paired sense promoter and the fold-decrease of sense transcription as already described (Figure S1A) (Schulz et al., 2013). AMRG are significantly more repressed than the Other Genes while the NRG present a mild phenotype. To directly assess nascent transcription, we took advantage of published datasets monitoring RNAPII PAR-CLIP in an Nrd1-AA strain (Schaughency et al., 2014). The same trend as obtained with the RNA-seq is observed implying that sense repression occurs at the nascent transcription level (Figure 1C) (Schaughency et al., 2014).

Since sense repression is transcriptional and related to the extension of antisense into the promoters, we investigated whether sense transcription initiation is affected upon antisense induction. To address this question, we performed Chromatin-Endogenous Cleavage (ChEC) of the TATA-Binding Protein (TBP, Spt15 in *S. cerevisiae*) in the Nrd1-AA strain treated or not with Rap in order to visualize PIC recruitment (Zentner et al., 2015). By ChEC, we observed the expected distribution of the PIC as peaks around the TATA (-like) Binding Sites (TBS) (Figure 1B) (Rhee and Pugh, 2012). Interestingly, AMRG present a stronger decrease in PIC binding upon antisense induction as compared to the Other Genes, while NRG again exhibit a milder phenotype (Figures 1D-1G and Figure S1C). The almost perfectly overlapping PIC peaks in -Rap/+Rap at the Other Genes demonstrate the precision of the measurement and validate the experimental accuracy.

Hence, as inferred by lower binding of the PIC at coding gene promoters, sense repression by antisense noncoding transcription occurs at the transcription initiation step.

Antisense induction into promoters increases nucleosome occupancy over the TBS through -1/+1 shifting

As mentioned above, antisense-mediated transcription interference involves a chromatin-based mechanism. An interesting scenario would be that nucleosomes repositioned over promoters upon antisense induction may compete with PIC binding. We investigated this possibility at near base-pair resolution by monitoring nucleosome positioning around TBSs by paired-end Micrococcal Nuclease-sequencing (MNase-seq) upon antisense elongation in +Rap (Figure 2A). To visualize the nucleosomes overlapping with the TBSs , we plotted nucleosome dyads and quantified the occupancy over a 100bp TBS-centered region. We detect a subtle but highly significant increase of nucleosome occupancy at the AMRG TBS as compared to the NRG and Other genes (Figures 2A, 2C, 2H and Figure S2A). To rule out the possibility that this measurement may be artifactual due to near-background values, we performed a complementary technique, Assay for Transposase-Accessible Chromatin-sequencing (ATAC-seq), to convert the "valley" signal into a "peak" signal, making this measurement more accurate. Similar to the MNase-seq, antisense induction into AMRG promoters significantly reduces the accessibility of the NDR (Figures 2B and 2C). Even <150bp NDRs, in which an additional nucleosome cannot fit, show this increase, suggesting that the occupancy increase may be the result of -1 and/or +1 sliding rather than incorporation of new nucleosomes (Figure 2D).

If -1 and/or +1 nucleosomes were sliding, one would expect a decrease of the occupancy when centering the analysis on their dyads (Figure 2E). This is what we observe for the -1 and +1 of AMRG upon antisense induction (Figures 2F, 2G and Figure S2B). This AMRG specific decrease is subtle in terms of fold-change but nicely anticorrelates with the fold-increase gained around TBSs. Importantly, when performing Chromatin ImmunoPrecipitation (ChIP) of H3 with sonicated extracts (with around 300 bp-resolution) at AMRG promoters, we do not detect any change in H3 content upon antisense induction, justifying the need of near base-pair resolution to visualize antisense-mediated chromatin changes (Figure S2C).

Altogether, these data suggest that antisense induction into AMRG promoters leads to -1/+1 nucleosome repositioning around the TBS thereby competing with the recruitment of the PIC.

H3K36me3 levels increase around AMRG TBSs upon antisense induction

Since H3K36me3 by the Set2 HMT is known to be involved in ncRNA-mediated transcription interference at several individual genes (du Mee et al., 2018; Kim et al., 2016; Nevers et al., 2018; van Werven et al., 2012), we analyzed this modification at nucleosome-resolution using MNase-ChIP-seq (Weiner et al., 2015). Upon antisense elongation, we detect an increase in H3K36me3 around TBSs but not when measuring at -1 and +1 nucleosome dyads (Figures 3A, 3B, 3D and Figures S3A and S3B). This increase in H3K36me3 is not biased towards large NDRs suggesting that this modification is linked to the sliding event and corresponds to a *de novo* modification induced by noncoding transcription entering into the NDR (Figure 3C). Accordingly, H3K36me3 ChIP at individual gene promoters indicates an increase of this modification at AMRG with longer incubation times in Rap, strengthening the model that antisense elongation into promoters induces *de novo* H3K36me3 deposition (Figure 3E).

Thus, the -1/+1 nucleosome repositioning correlates with the appearance of H3K36me3 around the TBS induced by antisense transcription, suggesting that newly-modified H3K36me3 nucleosomes undergo a sliding event.

H3K18ac and H4ac levels decrease at -1/+1 AMRG nucleosomes upon antisense induction

Histone deacetylases have previously been shown to be involved in antisense-mediated transcription interference (Camblong et al., 2007; Castelnuovo et al., 2013). Hence, we analyzed the H3K18ac modification landscape by MNase-ChIP-seq in the Nrd1-AA strain. In contrast to H3K36me3, H3K18ac levels specifically decrease at -1/+1 nucleosomes but do not change around the TBSs following antisense induction (Figures 4A-E and Figures S4A and S4B). The same results are observed when analyzing the H4ac modifications (Figures S4C and S4D).

Thus, H3K36me3 and H3K18ac/H4ac present an opposite pattern of changes. When H3K36me3 levels increase around the TBS, H3K18ac/H4ac levels decrease at -1/+1 nucleosomes. Since H3K36me3 is a platform to recruit a histone deacetylase and that H3K36me3 and H3K18ac/H4ac are highly anti-correlated, it is tempting to speculate that

antisense elongation into promoters may lead to H3K36me3 of the -1/+1 nucleosomes triggering deacetylation and subsequent sliding (Carrozza et al., 2005; Keogh et al., 2005; Sadeh et al., 2016; Weiner et al., 2015).

Loss of RSC binding at -1/+1 AMRG nucleosomes upon antisense induction

Considering the global role of the RSC chromatin remodeler in promoter NDR maintenance (Badis et al., 2008; Hartley and Madhani, 2009; Klein-Brill et al., 2019; Kubik et al., 2018; Yen et al., 2012), we asked whether nucleosome sliding was due to loss of RSC interaction with the NDR-flanking nucleosomes. This possibility is even more appealing when considering that the RSC complex interacts with acetylated histones *in vitro* through its multiple bromodomains (Chatterjee et al., 2011).

Consistently, when the recruitment of the Sth1 catalytic subunit of the RSC complex was examined by ChEC-seq in the Nrd1-AA strain, a specific loss of RSC interaction with -1 and +1 AMRG nucleosomes was detected in the presence of Rap (Figures 5A, 5B, 5C, 5D and Figures S5A and S5B). These observations suggest a link between the decreased acetylation of NDR-flanking nucleosomes and the loss of interaction with the essential RSC chromatin remodeler.

Loss of Rpd3 HDAC partially rescues transcription interference-associated phenotypes

If loss of -1/+1 acetylation directly affects RSC recruitment, a mutant in which the deacetylation step is defective may rescue RSC binding. This question was addressed by deletion of *RPD3* in the Ndr1-AA background. Rpd3 is the histone deacetylase component of the Rpd3S/L complex that maintains H3K18ac and H4ac levels low in the cell (Rundlett et al., 1996).

We first examined the fold-change in H3K18ac levels by ChIP upon antisense induction at selected AMRG promoters in presence or absence of Rpd3 (Figure S6A). As expected, upon Rap addition, *RPD*3 deletion leads to limited deacetylation of AMRG NDR-flanking nucleosomes as compared to the *WT* strain.

We then plotted the +Rap/-Rap fold-change of RSC binding at the +1 nucleosome, as assayed by Sth1 ChEC-seq (Figure 6A). When comparing to *WT* cells, we observe a partial rescue of RSC binding in *rpd3Δ* at AMRG. As RSC is essential for the maintenance of NDR opening (Badis et al., 2008; Hartley and Madhani, 2009; Klein-Brill et al., 2019; Kubik et al., 2018), the increased retention of RSC at AMRG -1/+1 nucleosomes in *rpd3Δ* may alleviate the

sliding event compared to *WT* cells. Indeed, as revealed by ATAC-seq, the increase in nucleosome occupancy around the TBS observed in *WT* cells upon antisense induction is partially rescued in *rpd3Δ* (Figure 6B). Consequently, loss of PIC binding and transcription interference at AMRG observed in *WT* are also alleviated in *rpd3Δ* (Figures 6C and 6D). Importantly, the level of antisense accumulation in AMRG is not globally affected in Nrd1-AA *Δrpd3* as compared to Nrd1-AA cells, indicating that the observed rescue is not an indirect effect of decreased antisense transcription (Figure S6B).

Thus, the acetylation level of -1/+1 nucleosomes appears as the central node of the transcription interference mechanism through its ability to recruit the RSC chromatin remodeler. Consequently, acetylation influences the accessibility of the PIC to the NDR and hence gene expression.

Model for antisense-mediated transcription interference in an inducible system and its genome-wide generalization at steady-state condition

Altogether, our results suggest the following model (Figure 7A). Under normal conditions (-Rap), noncoding transcription early termination prevents entry of antisense transcription into the NDR of promoters maintaining them open and favoring gene expression. When Nrd1 is anchored away, antisense elongation extends into the paired promoter NDR, resulting in H3K36me3 of the -1 and +1 nucleosomes, which are subsequently deacetylated through a process involving the Rpd3 HDAC. Loss of acetylation leads to decreased RSC recruitment and subsequent sliding of the -1/+1 nucleosomes towards the TBS. These events result in a steric hindrance for PIC binding and, consequently, in gene repression.

Our model is limited to only 4.5% of the genes in this non-physiological system to induce antisense elongation. Since antisense transcription can naturally extend into promoter NDRs depending on the strength of the noncoding transcription early termination process, we investigated whether our chromatin-based transcription interference model could be generalized under steady-state conditions. We ranked the coding genes into five quintiles according to the natural levels of nascent antisense transcription over their promoters (Figure 7B). The genes of the first quintile, presenting the highest levels of antisense transcription into promoters, are significantly less expressed than the ones of the other quintiles as assessed by RNA-seq and using nascent transcription data (Figure 7SA and Figure 7B). As predicted by our model, the first quintile shows increased nucleosome occupancy and increased H3K36me3 levels around the TBS (Figure 7C). Accordingly, the levels of H3K18ac, H4ac and RSC

binding at the -1 nucleosome appear as reduced in the first quintile compared to the others (Figures 7D and Figure S7B). Consistent with our model, in which H3K36me3-mediated deacetylation of NDR-flanking nucleosomes is involved in natural antisense-mediated transcription interference, the genes up-regulated in the absence of Rpd3 HDAC are significantly enriched in the first quintile (Figure 7E). Lastly, we analyzed the sensitivity of the different quintiles to RSC depletion known to induce global NDR shrinkage (Kubik et al., 2018). Analyses of published data show a global increase of nucleosome occupancy around the TBS for all the quintiles (Figure 7F) (Kubik et al., 2018). However, this increase is less important for the genes of the first quintile. Thus, as expected from our model, the genes showing the highest levels of antisense transcription into promoters are less sensitive to RSC depletion because they already present a higher nucleosome occupancy within the NDR at steady-state resulting from decreased interaction of the NDR-flanking nucleosomes with RSC.

Altogether, we propose that the chromatin-driven model of antisense-mediated transcription interference defined with a subset of genes in the inducible system can be extended with high significance up to 20% of the genes. These observations support the view that gene regulation through interleaved noncoding transcription is a major player of global chromatin shaping of promoters and gene expression in *S. cerevisiae*.

Discussion

A chromatin-driven transcription interference model derived from an antisense inducible system

Based on our results, we propose an antisense-mediated transcription interference mechanism through chromatin regulation (Figure 7A). The rescue of the different molecular phenotypes observed at AMRG in the absence of the Rpd3 HDAC enables us to validate such a chromatin-driven model (Figure 6). However, the rescue is only partial and other parameters have to be taken into consideration.

First antisense-mediated transcription interference may also implicate other HDACs as suggested by different earlier reports indicating the involvement of Set3 through recruitment by H3K4me2 or of Hda1 (Camblong et al., 2007; Kim et al., 2016; Kim et al., 2012). Another component of transcriptional interference may be the physical eviction of the sense PIC by the RNAPII travelling in antisense direction. However, we think this is unlikely since many DNA-binding proteins behave as roadblocking factors in front of which RNAPII stalls (Candelli et al., 2018a; Candelli et al., 2018b; Colin et al., 2014; Mayer et al., 2015). Nevertheless, the possibility of RNAPII removing DNA-binding factors remains to be thoroughly tested.

The fold-change obtained with the antisense inducible system for some of the molecular phenotypes are of low amplitude, albeit highly significant when comparing AMRG to Other genes. Yet, we do not expect drastic changes mainly because AMRG present relatively high levels of natural antisense transcription into promoters and are consequently already lowly expressed at steady state (Suppl. Figure 7C). Their chromatin is therefore already partially closed before antisense induction and Nrd1 anchor away only results in a subtle additional gain in repressive chromatin or a weak loss of active chromatin (Figures 1-5 and Figures S7D and S7E). Importantly, if we observe a magnitude of changes from 5-15% at the chromatin level for the AMRG (Figures 1-5), it ultimately leads to a 40% mRNA decrease as measured by RNA-seq (Figure S1A). Thus, low amplitude phenotypes at the chromatin level have important consequences on the cellular RNA content.

H3K36me3 and H3K18ac/H4ac nucleosomes are differently positioned

Induction of antisense into AMRG promoters leads to an increase in nucleosome occupancy around the TBS correlating with a loss of occupancy at -1/+1 (Figure 2). Concomitantly, H3K36me3 increases around the TBS while H3K18ac/H4ac marks are lost at

-1/+1 (Figures 3, 4 and Figure S4), strongly suggesting that these two mutually exclusive populations (Sadeh et al., 2016) are differently positioned. Based on these observations, we propose a simple model in which the transcription-associated H3K36 methylated nucleosomes prevent transcription initiation while acetylated nucleosomes are pushed aside allowing PIC binding. Thus, gene expression would depend on the metastable state of the promoter oscillating between a closed and open conformation. Antisense transcription frequency may promote NDR closing by modulating the H3K36me3 levels at NDR-flanking nucleosomes while histone demethylases, histone exchange or Histone Acetyl Transferases (HATs) may counteract the shrinkage. Similarly, such nucleosome movements are observed upon gene activation during the metabolic cycle when gene expression is synchronized (Nocetti and Whitehouse, 2016). According to our model, gene expression is maximal when -1/+1 nucleosomes are pushed aside in a movement mainly driven by H3K9ac and H3K18ac modifications (Hughes et al., 2012; Nocetti and Whitehouse, 2016; Sanchez-Gaya et al., 2018; Weiner et al., 2010).

Importantly, upon antisense induction, we also observe an increase in H3K36me3 occupancy at AMRG in between the +1/+2, +2/+3 and +3/+4 nucleosomes (Figure S3A) while deacetylation only occurs at the +2, +3 and +4 peaks (Figure S4A). Thus, the separation of H3K36me3/acetylated nucleosome populations is not restricted to promoters, but appears as a general feature along the yeast genome.

We did not detect a shift of the -1/+1 nucleosome peaks themselves upon antisense induction at AMRG (Figure 2F and Figure S2B), most likely because we are analyzing regions in which transcription occurs on both strands in the population but is dominated in frequency by sense transcription. Thus, nucleosome phasing is mainly dictated by sense transcription and the relative low frequency of antisense production only displaces a subpopulation and not the whole peaks. In other words, antisense induction may increase cell-to-cell variability in nucleosome positioning at AMRG promoters within a chromatin structure mainly imposed by sense transcription (Figure S7E). If we now consider the genes belonging to the Low antisense quintile (Figure 7), which are transcribed nearly exclusively in the sense orientation, we observe a clear shift of the H3K36me3 versus H3K18ac peaks over the coding region further supporting our model (Figure S7G).

Antisense-mediated transcription interference through chromatin regulation as a widespread mechanism of gene expression control in *S. cerevisiae*

Our results indicate that the top 20% of the genes showing the highest levels of antisense transcription into promoters are significantly less expressed than the others when taking into account nascent transcription data (Figure 7B). However, in agreement with published observations, the global anticorrelation between sense and antisense transcription is low (Figure S7F, Pearson correlation r=-0.13) (Brown et al., 2018; Murray et al., 2015). These analyses indicate that noncoding nascent transcription needs to reach a certain absolute level in the promoter NDR to induce transcription interference as already proposed by (Nevers et al., 2018) using RNA-seq data. When this level is reached, transcription into the promoter NDR becomes a dominant parameter, possibly through the chromatin rearrangement mechanism proposed here. Nevertheless, other parameters not considered in our study are likely to be involved, including different promoter sequences or transcription factors, the presence of roadblocking proteins or the recruitment of chromatin remodelers and histone modifiers.

We show that gene promoters with high levels of natural antisense tend to be more closed as compared to the others, a finding in agreement with published data (Dai and Dai, 2012; Murray et al., 2015). However, our results are in contradiction with the observation that high levels of antisense into promoters correlate with low levels of H3K36me3 and high levels of histone acetylation at promoters (Brown et al., 2018; Murray et al., 2015). This difference is mainly due to the normalization procedure as our nucleosome modification data were not normalized to H3 or MNase-seq levels. Considering the shape of the nucleosomal signal along the DNA, normalization in the "valley" region corresponding to the promoter is more sensitive to the background, increasing the probability of a biased result. Moreover, recent data have shown that one methylated H3K36 residue per nucleosome is sufficient to inhibit cryptic intragenic transcription indicating that the use of such a ratio may not be functionally relevant (Ichikawa et al., 2017).

The proposed model mainly considers antisense noncoding transcription, however a comparable transcription interference mechanism may take place as a result of upstream *in tandem* noncoding transcription overlapping with a downstream promoter. Indeed, based on the described involvement of both nucleosome positioning and H3K36me3 at specific loci (Hainer et al., 2011; Kim et al., 2016; Martens et al., 2004), our model may be relevant to transcription interference by noncoding transcription in a variety of configurations.

Importantly, our analyzes were only performed in rich medium. Early termination of lncRNA can be regulated in response to growth conditions leading to different patterns of noncoding transcription elongation (Bresson et al., 2017; Creamer et al., 2011; van Nues et al., 2017). Thus, a different framework of transcription interference may be expected depending on external conditions.

It is worth noting that about a hundred coding genes are less expressed in mRNA orientation than in lncRNA orientation at the nascent transcription level (data not shown). Thus, in some cases, the mRNA may appear as the intragenic transcript of the lncRNA. This concept, even if marginal in proportion, perfectly illustrates the plasticity of transcriptional circuits. RNAPII transcription happens all along the genome and evolution may shape the balance between expression noise and functionality (Struhl, 2007).

A common model for all eukaryotic NDRs?

In *S. cerevisiae*, NDRs are also regions where replication initiates, mainly through the accessibility of the Origin Recognition Complex (ORC) to the ARS (Autonomously Replicating Sequence) Consensus Sequence (ACS) (Eaton et al., 2010; Lai and Pugh, 2017). We recently showed that noncoding transcription entering into an ARS NDR is able to influence replication initiation by closing the NDR through increased nucleosome occupancy, as well as elevated H3K36me3 and decreased H3K18ac (Soudet et al., 2018). Importantly, replication defects induced by noncoding transcription readthrough into ARS NDR can be partially rescued in the absence of Set2. Although we did not have a precise mechanism in our previous study, the similarity between these earlier and the current observations tend to converge to a unique model that may be applicable to all types of NDRs.

Such a general mechanism may also be relevant to higher eukaryotes. Interestingly, in mammalian cells, replication mainly initiates within gene promoters (Chen et al., 2019; Miotto et al., 2016; Sequeira-Mendes et al., 2009). Replication initiation efficiency nicely correlates with transcription initiation strength, which itself correlates with the accessibility of the NDR (Brown et al., 2018; Chen et al., 2019). Similarly to yeast cells, high levels of antisense lncRNAs over promoter NDRs correlate with a transcription interference phenotype and a closed NDR conformation (Brown et al., 2018; Chen et al., 2016). Together, these observations suggest that noncoding transcription readthrough into NDRs may be a neglected parameter regulating both replication initiation and gene expression in mammalian cells through a chromatin-driven mechanism. It would therefore also be of interest to analyze the

consequences of noncoding transcription readthrough on the chromatin structure of enhancers which also correspond to NDRs. High resolution maps of nucleosomes and histone modifications will reveal whether the proposed chromatin-driven model can be extended to mammalian cells.

Acknowledgements

We thank Benjamin Albert, Guillaume Canal, Charlie Rochat, Florian Steiner, Michel Strubin and all members of the Stutz laboratory for critical reading of the manuscript, comments and discussions. We thank Mylene Docquier and the iGE3 genomics platform of the University of Geneva for performing all the deep sequencing. This work was supported by funds from the Swiss National Science Foundation (grants 31003A 153331 and 31003A_182344 to F.S.), iGE3 and the Canton of Geneva.

Author Contributions

Conceptualization: F.S., J.S. Investigation: J.K.G, A.M., V.G.M., J.S. Formal Analysis: J.K.G, J.S. Data Curation: J.S. Writing – Original Draft: J.S. Writing – Review and Editing: J.K.G., F.S., J.S. Supervision: F.S., J.S. Funding acquisition: F.S.

Declaration of interests

Authors declare no competing interests.

References

Afgan, E., Baker, D., Batut, B., van den Beek, M., Bouvier, D., Cech, M., Chilton, J., Clements, D., Coraor, N., Gruning, B.A., *et al.* (2018). The Galaxy platform for accessible, reproducible and collaborative biomedical analyses: 2018 update. Nucleic Acids Res *46*, W537-W544.

Au - Grbesa, I., Au - Tannenbaum, M., Au - Sarusi-Portuguez, A., Au - Schwartz, M., and Au - Hakim, O. (2017). Mapping Genome-wide Accessible Chromatin in Primary Human T Lymphocytes by ATAC-Seq. JoVE, e56313.

Badis, G., Chan, E.T., van Bakel, H., Pena-Castillo, L., Tillo, D., Tsui, K., Carlson, C.D., Gossett, A.J., Hasinoff, M.J., Warren, C.L., *et al.* (2008). A library of yeast transcription factor motifs reveals a widespread function for Rsc3 in targeting nucleosome exclusion at promoters. Mol Cell *32*, 878-887.

Brahma, S., and Henikoff, S. (2019). RSC-Associated Subnucleosomes Define MNase-Sensitive Promoters in Yeast. Mol Cell *73*, 238-249 e233.

Bresson, S., Tuck, A., Staneva, D., and Tollervey, D. (2017). Nuclear RNA Decay Pathways Aid Rapid Remodeling of Gene Expression in Yeast. Mol Cell *65*, 787-800 e785.

Brown, T., Howe, F.S., Murray, S.C., Wouters, M., Lorenz, P., Seward, E., Rata, S., Angel, A., and Mellor, J. (2018). Antisense transcription-dependent chromatin signature modulates sense transcript dynamics. Mol Syst Biol *14*, e8007.

Buenrostro, J.D., Giresi, P.G., Zaba, L.C., Chang, H.Y., and Greenleaf, W.J. (2013). Transposition of native chromatin for fast and sensitive epigenomic profiling of open chromatin, DNA-binding proteins and nucleosome position. Nat Methods *10*, 1213-1218.

Buenrostro, J.D., Wu, B., Chang, H.Y., and Greenleaf, W.J. (2015). ATAC-seq: A Method for Assaying Chromatin Accessibility Genome-Wide. Curr Protoc Mol Biol *109*, 21 29 21-29.

Camblong, J., Iglesias, N., Fickentscher, C., Dieppois, G., and Stutz, F. (2007). Antisense RNA stabilization induces transcriptional gene silencing via histone deacetylation in S. cerevisiae. Cell *131*, 706-717.

Candelli, T., Challal, D., Briand, J.B., Boulay, J., Porrua, O., Colin, J., and Libri, D. (2018a). High-resolution transcription maps reveal the widespread impact of roadblock termination in yeast. EMBO J *37*.

Candelli, T., Gros, J., and Libri, D. (2018b). Pervasive transcription fine-tunes replication origin activity. Elife *7*.

Carrozza, M.J., Li, B., Florens, L., Suganuma, T., Swanson, S.K., Lee, K.K., Shia, W.J., Anderson, S., Yates, J., Washburn, M.P., *et al.* (2005). Histone H3 methylation by Set2 directs deacetylation of coding regions by Rpd3S to suppress spurious intragenic transcription. Cell *123*, 581-592.

Castelnuovo, M., Rahman, S., Guffanti, E., Infantino, V., Stutz, F., and Zenklusen, D. (2013). Bimodal expression of PHO84 is modulated by early termination of antisense transcription. Nat Struct Mol Biol *20*, 851-858.

Castelnuovo, M., Zaugg, J.B., Guffanti, E., Maffioletti, A., Camblong, J., Xu, Z., Clauder-Munster, S., Steinmetz, L.M., Luscombe, N.M., and Stutz, F. (2014). Role of histone modifications and early termination in pervasive transcription and antisense-mediated gene silencing in yeast. Nucleic Acids Res *42*, 4348-4362.

Chatterjee, N., Sinha, D., Lemma-Dechassa, M., Tan, S., Shogren-Knaak, M.A., and Bartholomew, B. (2011). Histone H3 tail acetylation modulates ATP-dependent remodeling through multiple mechanisms. Nucleic Acids Res *39*, 8378-8391.

Chen, K., Xi, Y., Pan, X., Li, Z., Kaestner, K., Tyler, J., Dent, S., He, X., and Li, W. (2013). DANPOS: dynamic analysis of nucleosome position and occupancy by sequencing. Genome Res *23*, 341-351.

Chen, Y., Pai, A.A., Herudek, J., Lubas, M., Meola, N., Jarvelin, A.I., Andersson, R., Pelechano, V., Steinmetz, L.M., Jensen, T.H., *et al.* (2016). Principles for RNA metabolism and alternative transcription initiation within closely spaced promoters. Nat Genet *48*, 984-994.

Chen, Y.H., Keegan, S., Kahli, M., Tonzi, P., Fenyo, D., Huang, T.T., and Smith, D.J. (2019). Transcription shapes DNA replication initiation and termination in human cells. Nat Struct Mol Biol *26*, 67-77.

Chereji, R.V., Ramachandran, S., Bryson, T.D., and Henikoff, S. (2018). Precise genome-wide mapping of single nucleosomes and linkers in vivo. Genome Biol *19*, 19.

Churchman, L.S., and Weissman, J.S. (2011). Nascent transcript sequencing visualizes transcription at nucleotide resolution. Nature *469*, 368-373.

Colin, J., Candelli, T., Porrua, O., Boulay, J., Zhu, C., Lacroute, F., Steinmetz, L.M., and Libri, D. (2014). Roadblock termination by reb1p restricts cryptic and readthrough transcription. Mol Cell *56*, 667-680.

Core, L.J., Waterfall, J.J., and Lis, J.T. (2008). Nascent RNA sequencing reveals widespread pausing and divergent initiation at human promoters. Science *322*, 1845-1848.

Creamer, T.J., Darby, M.M., Jamonnak, N., Schaughency, P., Hao, H., Wheelan, S.J., and Corden, J.L. (2011). Transcriptome-wide binding sites for components of the Saccharomyces cerevisiae non-poly(A) termination pathway: Nrd1, Nab3, and Sen1. PLoS Genet *7*, e1002329.

Dai, Z., and Dai, X. (2012). Antisense transcription is coupled to nucleosome occupancy in sense promoters. Bioinformatics *28*, 2719-2723.

Djebali, S., Davis, C.A., Merkel, A., Dobin, A., Lassmann, T., Mortazavi, A., Tanzer, A., Lagarde, J., Lin, W., Schlesinger, F., *et al.* (2012). Landscape of transcription in human cells. Nature *489*, 101-108.

du Mee, D.J.M., Ivanov, M., Parker, J.P., Buratowski, S., and Marquardt, S. (2018). Efficient termination of nuclear lncRNA transcription promotes mitochondrial genome maintenance. Elife *7*.

Eaton, M.L., Galani, K., Kang, S., Bell, S.P., and MacAlpine, D.M. (2010). Conserved nucleosome positioning defines replication origins. Genes Dev *24*, 748-753.

Fischl, H., Howe, F.S., Furger, A., and Mellor, J. (2017). Paf1 Has Distinct Roles in Transcription Elongation and Differential Transcript Fate. Mol Cell *65*, 685-698 e688.

Hainer, S.J., Pruneski, J.A., Mitchell, R.D., Monteverde, R.M., and Martens, J.A. (2011). Intergenic transcription causes repression by directing nucleosome assembly. Genes Dev *25*, 29-40.

Hartley, P.D., and Madhani, H.D. (2009). Mechanisms that specify promoter nucleosome location and identity. Cell *137*, 445-458.

Haruki, H., Nishikawa, J., and Laemmli, U.K. (2008). The anchor-away technique: rapid, conditional establishment of yeast mutant phenotypes. Mol Cell *31*, 925-932.

Hughes, A.L., Jin, Y., Rando, O.J., and Struhl, K. (2012). A functional evolutionary approach to identify determinants of nucleosome positioning: a unifying model for establishing the genome-wide pattern. Mol Cell *48*, 5-15.

Ichikawa, Y., Connelly, C.F., Appleboim, A., Miller, T.C., Jacobi, H., Abshiru, N.A., Chou, H.J., Chen, Y., Sharma, U., Zheng, Y., *et al.* (2017). A synthetic biology approach to probing nucleosome symmetry. Elife *6*.

Jensen, T.H., Jacquier, A., and Libri, D. (2013). Dealing with pervasive transcription. Mol Cell *52*, 473-484.

Joshi, A.A., and Struhl, K. (2005). Eaf3 chromodomain interaction with methylated H3-K36 links histone deacetylation to Pol II elongation. Mol Cell *20*, 971-978.

Kaikkonen, M.U., and Adelman, K. (2018). Emerging Roles of Non-Coding RNA Transcription. Trends Biochem Sci *43*, 654-667.

Keogh, M.C., Kurdistani, S.K., Morris, S.A., Ahn, S.H., Podolny, V., Collins, S.R., Schuldiner, M., Chin, K., Punna, T., Thompson, N.J., *et al.* (2005). Cotranscriptional set2 methylation of histone H3 lysine 36 recruits a repressive Rpd3 complex. Cell *123*, 593-605.

Kim, J.H., Lee, B.B., Oh, Y.M., Zhu, C., Steinmetz, L.M., Lee, Y., Kim, W.K., Lee, S.B., Buratowski, S., and Kim, T. (2016). Modulation of mRNA and lncRNA expression dynamics by the Set2-Rpd3S pathway. Nat Commun *7*, 13534.

Kim, T., Xu, Z., Clauder-Munster, S., Steinmetz, L.M., and Buratowski, S. (2012). Set3 HDAC mediates effects of overlapping noncoding transcription on gene induction kinetics. Cell *150*, 1158-1169.

Klein-Brill, A., Joseph-Strauss, D., Appleboim, A., and Friedman, N. (2019). Dynamics of Chromatin and Transcription during Transient Depletion of the RSC Chromatin Remodeling Complex. Cell Rep *26*, 279-292 e275.

Kubik, S., Bruzzone, M.J., Jacquet, P., Falcone, J.L., Rougemont, J., and Shore, D. (2015). Nucleosome Stability Distinguishes Two Different Promoter Types at All Protein-Coding Genes in Yeast. Mol Cell *60*, 422-434.

Kubik, S., O'Duibhir, E., de Jonge, W.J., Mattarocci, S., Albert, B., Falcone, J.L., Bruzzone, M.J., Holstege, F.C.P., and Shore, D. (2018). Sequence-Directed Action of RSC Remodeler and General Regulatory Factors Modulates +1 Nucleosome Position to Facilitate Transcription. Mol Cell *71*, 89-102 e105.

Kuras, L., and Struhl, K. (1999). Binding of TBP to promoters in vivo is stimulated by activators and requires Pol II holoenzyme. Nature *399*, 609-613.

Lai, W.K.M., and Pugh, B.F. (2017). Understanding nucleosome dynamics and their links to gene expression and DNA replication. Nat Rev Mol Cell Biol *18*, 548-562.

Langmead, B., and Salzberg, S.L. (2012). Fast gapped-read alignment with Bowtie 2. Nat Methods *9*, 357-359.

Langmead, B., Trapnell, C., Pop, M., and Salzberg, S.L. (2009). Ultrafast and memory-efficient alignment of short DNA sequences to the human genome. Genome Biol *10*, R25.

Li, B., Howe, L., Anderson, S., Yates, J.R., 3rd, and Workman, J.L. (2003). The Set2 histone methyltransferase functions through the phosphorylated carboxyl-terminal domain of RNA polymerase II. J Biol Chem *278*, 8897-8903.

Malabat, C., Feuerbach, F., Ma, L., Saveanu, C., and Jacquier, A. (2015). Quality control of transcription start site selection by nonsense-mediated-mRNA decay. Elife *4*.

Martens, J.A., Laprade, L., and Winston, F. (2004). Intergenic transcription is required to repress the Saccharomyces cerevisiae SER3 gene. Nature *429*, 571-574.

Mayer, A., di Iulio, J., Maleri, S., Eser, U., Vierstra, J., Reynolds, A., Sandstrom, R., Stamatoyannopoulos, J.A., and Churchman, L.S. (2015). Native elongating transcript sequencing reveals human transcriptional activity at nucleotide resolution. Cell *161*, 541-554.

Mellor, J., Woloszczuk, R., and Howe, F.S. (2016). The Interleaved Genome. Trends Genet *32*, 57-71.

Miotto, B., Ji, Z., and Struhl, K. (2016). Selectivity of ORC binding sites and the relation to replication timing, fragile sites, and deletions in cancers. Proc Natl Acad Sci U S A *113*, E4810-4819.

Murray, S.C., Haenni, S., Howe, F.S., Fischl, H., Chocian, K., Nair, A., and Mellor, J. (2015). Sense and antisense transcription are associated with distinct chromatin architectures across genes. Nucleic Acids Res *43*, 7823-7837.

Neil, H., Malabat, C., d'Aubenton-Carafa, Y., Xu, Z., Steinmetz, L.M., and Jacquier, A. (2009). Widespread bidirectional promoters are the major source of cryptic transcripts in yeast. Nature *457*, 1038-1042.

Nevers, A., Doyen, A., Malabat, C., Neron, B., Kergrohen, T., Jacquier, A., and Badis, G. (2018). Antisense transcriptional interference mediates condition-specific gene repression in budding yeast. Nucleic Acids Res *46*, 6009-6025.

Nocetti, N., and Whitehouse, I. (2016). Nucleosome repositioning underlies dynamic gene expression. Genes Dev *30*, 660-672.

Nojima, T., Gomes, T., Grosso, A.R.F., Kimura, H., Dye, M.J., Dhir, S., Carmo-Fonseca, M., and Proudfoot, N.J. (2015). Mammalian NET-Seq Reveals Genome-wide Nascent Transcription Coupled to RNA Processing. Cell *161*, 526-540.

Porrua, O., and Libri, D. (2015). Transcription termination and the control of the transcriptome: why, where and how to stop. Nat Rev Mol Cell Biol *16*, 190-202.

Proudfoot, N.J. (1986). Transcriptional interference and termination between duplicated alpha-globin gene constructs suggests a novel mechanism for gene regulation. Nature *322*, 562-565.

Ramirez, F., Ryan, D.P., Gruning, B., Bhardwaj, V., Kilpert, F., Richter, A.S., Heyne, S., Dundar, F., and Manke, T. (2016). deepTools2: a next generation web server for deep-sequencing data analysis. Nucleic Acids Res *44*, W160-165.

Rando, O.J., and Winston, F. (2012). Chromatin and transcription in yeast. Genetics *190*, 351-387.

Rhee, H.S., and Pugh, B.F. (2012). Genome-wide structure and organization of eukaryotic pre-initiation complexes. Nature *483*, 295-301.

Rundlett, S.E., Carmen, A.A., Kobayashi, R., Bavykin, S., Turner, B.M., and Grunstein, M. (1996). HDA1 and RPD3 are members of distinct yeast histone deacetylase complexes that regulate silencing and transcription. Proc Natl Acad Sci U S A *93*, 14503-14508.

Sadeh, R., Launer-Wachs, R., Wandel, H., Rahat, A., and Friedman, N. (2016). Elucidating Combinatorial Chromatin States at Single-Nucleosome Resolution. Mol Cell *63*, 1080-1088.

Sanchez-Gaya, V., Casani-Galdon, S., Ugidos, M., Kuang, Z., Mellor, J., Conesa, A., and Tarazona, S. (2018). Elucidating the Role of Chromatin State and Transcription Factors on the Regulation of the Yeast Metabolic Cycle: A Multi-Omic Integrative Approach. Front Genet *9*, 578.

Schaughency, P., Merran, J., and Corden, J.L. (2014). Genome-wide mapping of yeast RNA polymerase II termination. PLoS Genet *10*, e1004632.

Schep, A.N., Buenrostro, J.D., Denny, S.K., Schwartz, K., Sherlock, G., and Greenleaf, W.J. (2015). Structured nucleosome fingerprints enable high-resolution mapping of chromatin architecture within regulatory regions. Genome Res *25*, 1757-1770.

Schulz, D., Schwalb, B., Kiesel, A., Baejen, C., Torkler, P., Gagneur, J., Soeding, J., and Cramer, P. (2013). Transcriptome surveillance by selective termination of noncoding RNA synthesis. Cell *155*, 1075-1087.

Sequeira-Mendes, J., Diaz-Uriarte, R., Apedaile, A., Huntley, D., Brockdorff, N., and Gomez, M. (2009). Transcription initiation activity sets replication origin efficiency in mammalian cells. PLoS Genet *5*, e1000446.

Soudet, J., Gill, J.K., and Stutz, F. (2018). Noncoding transcription influences the replication initiation program through chromatin regulation. Genome Res *28*, 1882-1893.

Strahl-Bolsinger, S., Hecht, A., Luo, K., and Grunstein, M. (1997). SIR2 and SIR4 interactions differ in core and extended telomeric heterochromatin in yeast. Genes Dev *11*, 83-93.

Struhl, K. (2007). Transcriptional noise and the fidelity of initiation by RNA polymerase II. Nat Struct Mol Biol *14*, 103-105.

van Dijk, E.L., Chen, C.L., d'Aubenton-Carafa, Y., Gourvennec, S., Kwapisz, M., Roche, V., Bertrand, C., Silvain, M., Legoix-Ne, P., Loeillet, S.*, et al.* (2011). XUTs are a class of Xrn1-sensitive antisense regulatory non-coding RNA in yeast. Nature *475*, 114-117.

van Nues, R., Schweikert, G., de Leau, E., Selega, A., Langford, A., Franklin, R., Iosub, I., Wadsworth, P., Sanguinetti, G., and Granneman, S. (2017). Kinetic CRAC uncovers a role for Nab3 in determining gene expression profiles during stress. Nat Commun *8*, 12.

van Werven, F.J., Neuert, G., Hendrick, N., Lardenois, A., Buratowski, S., van Oudenaarden, A., Primig, M., and Amon, A. (2012). Transcription of two long noncoding RNAs mediates mating-type control of gametogenesis in budding yeast. Cell *150*, 1170-1181.

Venkatesh, S., Smolle, M., Li, H., Gogol, M.M., Saint, M., Kumar, S., Natarajan, K., and Workman, J.L. (2012). Set2 methylation of histone H3 lysine 36 suppresses histone exchange on transcribed genes. Nature *489*, 452-455.

Venkatesh, S., and Workman, J.L. (2015). Histone exchange, chromatin structure and the regulation of transcription. Nat Rev Mol Cell Biol *16*, 178-189.

Weiner, A., Hsieh, T.H., Appleboim, A., Chen, H.V., Rahat, A., Amit, I., Rando, O.J., and Friedman, N. (2015). High-resolution chromatin dynamics during a yeast stress response. Mol Cell *58*, 371-386.

Weiner, A., Hughes, A., Yassour, M., Rando, O.J., and Friedman, N. (2010). High-resolution nucleosome mapping reveals transcription-dependent promoter packaging. Genome Res *20*, 90-100.

Wery, M., Gautier, C., Descrimes, M., Yoda, M., Vennin-Rendos, H., Migeot, V., Gautheret, D., Hermand, D., and Morillon, A. (2018). Native elongating transcript sequencing reveals global anti-correlation between sense and antisense nascent transcription in fission yeast. RNA *24*, 196-208.

Xu, Z., Wei, W., Gagneur, J., Perocchi, F., Clauder-Munster, S., Camblong, J., Guffanti, E., Stutz, F., Huber, W., and Steinmetz, L.M. (2009). Bidirectional promoters generate pervasive transcription in yeast. Nature *457*, 1033-1037.

Yen, K., Vinayachandran, V., Batta, K., Koerber, R.T., and Pugh, B.F. (2012). Genome-wide nucleosome specificity and directionality of chromatin remodelers. Cell *149*, 1461-1473.

Zentner, G.E., and Henikoff, S. (2013). Regulation of nucleosome dynamics by histone modifications. Nat Struct Mol Biol *20*, 259-266.

Zentner, G.E., Kasinathan, S., Xin, B., Rohs, R., and Henikoff, S. (2015). ChEC-seq kinetics discriminates transcription factor binding sites by DNA sequence and shape in vivo. Nat Commun *6*, 8733.

Figure Legends

Figure 1. Antisense-mediated transcription interference decreases PIC binding.

(A) Scatter dot-plot of the Nrd1-AA RNA-seq. Nrd1-AA cells were treated or not with Rapamycin (Rap) for 1h before RNA extraction. Results are represented in log2 of Reads Per Kilobase of transcript per Million mapped reads (rpkm) in both antisense and sense orientation. DESeq was used to define the different gene classes (see Method details).

(B) Snapshot of the Nrd1-AA RNA-seq depicting a locus containing both an AMRG (*VAC7*) and a NRG (*MSG5*). Antisense induction in +Rap leads to the elongation of *NUT1367* noncoding RNA into the *VAC7* promoter and to the subsequent transcription interference of the *VAC7* transcript.

(C) Box-plots indicating the RNAPII PAR-CLIP fold-change (+Rap/-Rap) in an Nrd1-AA strain. Data were taken from (Schaughency et al., 2014). Antisense transcription was measured over the -100bp to TSS of the paired sense, and sense transcription was examined over 100bp upstream of the polyA site.

(D) Metagene analyses of TBP-ChEC induced for 30sec in an Nrd1-AA strain treated or not with Rap for 1h. The grey box represents the 100bp TBS-centered area over which statistics are generated. The center of 0-120bp paired-end fragments is represented for the plots and statistical analyses.

(E) Metagene analysis and heatmap depicting the +Rap/-Rap fold-change (log2) of the TBP-ChEC at AMRG and NRG promoters.

(F) Box-plots indicating the +Rap/-Rap fold-change (log2) of TBP-ChEC in the Nrd1-AA strain as measured over the 100bp area centered on the TBS.

(G) Snapshot depicting the AMRG-class coding gene *VAC7* repressed in +Rap by induction of *NUT1367* antisense transcription. The rectangle highlights the PIC involved in *VAC7* transcription.

Figure 2. Antisense induction leads to paired sense promoter closing.

(A) Aggregate plots centered on TBSs of MNase-seq profiles obtained in an Nrd1-AA strain treated or not for 1h with Rap. The centers of 120-200bp paired-end fragments are represented. The 100bp TBS-centered area represented as a grey rectangle corresponds to the zone in which nucleosomes can virtually overlap with the TBS.

(B) Metagene analyses of ATAC-seq in an Nrd1-AA strain treated or not for 1h with Rap. The centers of 0-120bp paired-end fragments are depicted.

(C) Box-plots indicating the +Rap/-Rap fold-change (log2) of dyads occupancy and NDR opening obtained through MNase-seq and ATAC-seq respectively. Statistics are generated over the 100bp TBS-centered area.

(D) Heatmaps centered on the +1 nucleosome of MNase-seq signal in -Rap (top) and MNase-seq +Rap/-Rap fold-change (log2) (bottom) for the AMRG. NDRs were ranked according to their length to discriminate between "Wide" NDRs, in which additional nucleosomes can virtually accommodate, and "Narrow" NDRs that cannot fit a 150bp DNA-covered nucleosome.

(E) Cartoon depicting that gain of nucleosomes around the TBSs through sliding should be accompanied by -1 and /or +1 decrease in dyads occupancy peaks.

(F) Aggregate plots aligned on the -1 dyads of MNase-seq profiles obtained in an Nrd1-AA strain treated or not for 1h with Rapamycin. The grey box represents the 20bp -1 nucleosome-centered area over which statistics are generated.

(G) Box-plots representing the dyad occupancy +Rap/-Rap fold-change (log2) over a 20bp area centered on the -1 and +1 nucleosomes respectively.

(H) Snapshot of both MNase-seq and ATAC-seq profiles at the AMRG *VAC7*. The NDR from which *VAC7* transcription is initiated is highlighted by a rectangle.

Figure 3. H3K36me3 levels increase around TBS upon antisense induction.

(A) Metagene profiles of H3K36me3 MNase-ChIP-seq levels centered on TBSs and -1 nucleosome dyad obtained in an Nrd1-AA strain treated or not for 1h with Rap. The centers of 120-200bp paired-end fragments are represented here. The grey boxes represent the 100bp TBS- and the 20bp -1 nucleosome-centered areas respectively.

(B) Box-plots indicating the +Rap/-Rap fold-change (log2) of increase in H3K36me3 levels over the 100bp TBS- and 20bp -1/+1 nucleosomes-centered areas.

(C) Heatmaps centered on the +1 nucleosome as in **Figure 2D**.

(D) Snapshot of H3K36me3 MNase-ChIP-seq levels at the AMRG *VAC7*. The NDR of *VAC7* is highlighted by a rectangle.

(E) ChIP of H3K36me3 histone modification at gene promoters of AMRG, NRG and Other genes. ChIPs were performed at 0, 30, 60, 90 and 120min after rapamycin addition. Immunoprecipitated promoter NDRs were normalized to immunoprecipitated *SPT15* ORF

after qPCR amplification. Primers were designed to target each promoter NDR. The fold-change was artificially set to 1 for each gene in the -Rap condition. Error bars represent the Standard Error of the Mean (SEM) for a set of 3 independent experiments.

Figure 4. Antisense elongation into AMRG promoters leads to decreased H3K18ac levels at -1/+1 nucleosomes.

(A) Metagene profiles of H3K18ac MNase-ChIP-seq reads centered on TBSs and -1 dyad midpoint in an Nrd1-AA strain treated or not for 1h with Rap. The centers of 120-200bp paired-end fragments are represented here. The grey boxes represent the 100bp and 20bp areas centered on the TBS and -1 nucleosome respectively.
(B) Box-plots indicating the +Rap/-Rap fold-change (log2) in H3K18ac levels over the 100bp TBS- and 20bp -1/+1-centered areas.
(C) Metagene plots and heatmaps centered on the -1 nucleosome indicating the fold-change of H3K18ac for both AMRG and NRG around the -1 nucleosome.
(D) Snapshot of H3K18ac MNase-ChIP-seq levels at the AMRG *VAC7*. The -1/+1 nucleosomes of *VAC7* are highlighted by a rectangle.
(E) ChIP of H3K18ac at gene promoters of AMRG, NRG and Other genes (n=3) normalized as in **Figure 3E**.

Figure 5. RSC interaction with -1/+1 nucleosomes decreases upon antisense induction.

(A) Metagene profiles of Sth1-ChEC in an Nrd1-AA strain treated or not for 1h with Rap around the TBS and -1 nucleosome. The centers of 120-200bp fragments are represented here in order to get rid of the RSC-associated Fragile-Nucleosome population covering <120bp area (Brahma and Henikoff, 2019; Kubik et al., 2015). The grey boxes represent the 100bp and 20bp areas centered around the TBS and the -1 nucleosome respectively.
(B) Box-plots indicating the +Rap/-Rap fold-change (log2) of increase in Sth1-ChEC levels over the 100bp TBS- and 20bp -1/+1-centered areas.
(C) Aggregate plots and heatmaps centered on the -1 nucleosome indicating the Sth1-ChEC fold-change for both AMRG and NRG around the -1 nucleosome.
(D) Snapshot of Sth1-ChEC levels at the AMRG *VAC7*. The -1/+1 nucleosomes are highlighted by a rectangle.

Figure 6. Loss of the Rpd3 HDAC partially rescues antisense-mediated gene repression phenotypes.

(A) (B) (C) (D) Box-plots indicating the normalized log2 fold-change (+Rap/-Rap) for Sth1 ChEC-seq, ATAC-seq, TBP ChEC-seq and RNA-seq in an Nrd1-AA strain as compared to Nrd1-AA *rpd3Δ* cells. Plots for the Nrd1-AA strain are already presented in Figures 5B, 2C, 1F and Figure S1C with the exception of the normalized fold-change, for which calculation is described in Method details.

Figure 7. Model of induced chromatin-driven transcription interference and its generalization in the steady-state genome.

(A) Model of antisense-mediated transcription interference through promoter chromatin regulation. For a description of the model, see the Results section.
(B) Left panel: Box-plots defining the five quintiles according to their natural level of nascent antisense transcription into gene promoters (-100 to TSS area). Each quintile contains 955 genes. RNA PolII PAR-CLIP data were taken from (Schaughency et al., 2014). Right panel: Box-plots depicting levels of nascent coding sense transcription in an area of 100bp upstream of the polyA site.
(C) Aggregate plot of nucleosome occupancy and H3K36me3 levels around the TBS with respect to the different quintiles.
(D) Metagene analysis of H3K18ac (top) and RSC binding (bottom) levels around -1 nucleosome according to the different quintiles.
(E) Percentage of genes from each quintile upregulated in a *rpd3Δ* strain (>2fold). Significance was defined according to a hypergeometrical test.
(F) Box-plot of nucleosome occupancy fold-change in a 50bp-TBS centered region upon anchor-away of Sth1 for 1h. Data were retrieved from (Kubik et al., 2018).

STAR Methods

Contact for reagent and resource sharing

Further information and requests for resources and reagents should be directed to and will be fulfilled by the Lead Contact, Julien Soudet (julien.soudet@unige.ch).

Experimental model

Saccharomyces cerevisiae strains and growth

All strains were derived from the Anchor-Away genetic backgrounds (see Supplemental Table 1) (Haruki et al. 2008). Cells were grown in YEPD medium (1% yeast extract, 1% peptone) supplemented with 2% glucose as carbon source. All strains were grown at 30°C and were not affected in growth by the different tags or deletions (Supplemental Table 1). Anchor-away of Nrd1-AA was induced by adding 1µg/ml of rapamycin to the medium.

Method details

RNA extraction and RNA-seq

RNAs were extracted using Glass-beads and TRIzol (Invitrogen). RNA library preparation and single-end stranded sequencing were performed at the IGE3 genomics platform of the University of Geneva.

MNase(-ChIP)-seq

The MNase- and MNase-ChIP-seq experiments were performed mainly as described in (Weiner et al., 2015) with the following modifications. Nrd1-AA strain was inoculated overnight and diluted in the morning to OD_{600}=0.2 in YEPD medium. Yeast cell cultures of 100 ml was used per modification. Rapamycin treatment was performed at OD_{600}=0.5 for 60 minutes on half of the culture. The cells were fixed with formaldehyde at a final concentration of 1% for 15 minutes followed by glycine addition at a final concentration of 125 mM for 5 minutes. Cells were washed 2x with ddH_2O, harvested in magnaLyser tubes (Roche) (100 mL cell culture/tube) and frozen at -20°C .

Chromatin extraction was performed by breaking cells in 1 mL of Cell Breaking buffer (0.1 M Tris-HCl, pH 7.9, 20% glycerol, EDTA-free protease inhibitors) and 1 mL of acid-washed glass beads in a magnaLyser (Roche). The cell extract was then centrifuged at 19,000g at 4 °C for 10 minutes to collect chromatin. The chromatin was resuspended in 600 µL of NP buffer (0.5 mM Spermidine, 50 mM NaCl, 1mM β-mercaptoethanol, 0.075% NP-40, 10 mM Tris-HCl pH 7.4, 5 mM $MgCl_2$, 1 mM $CaCl_2$) per tube. The DNA concentration was measured using Qubit dsDNA BR assay kit (Invitrogen). Chromatin was diluted to 20 µg/mL using NP buffer in all conditions for comparable results.

MNase treatment was performed using 0.2 µL of MNase (ThermoScientific 100 units/µL) / 12 µg of chromatin in 600 µL reaction mixture for 14 minutes at 37 °C. To perform all the modifications for one replicate from one cell culture the reaction was scaled 10x. The reaction was stopped by adding EDTA (final concentration 20 mM) in the reaction mixture.

For MNase-seq, an equal amount of elution buffer (10 mM Tris-HCl, pH 8.0, 1% SDS, 150 mM NaCl, 5 mM DTT) was added. The further steps for MNase-seq are same as the ones performed after MNase-ChIP elution.

For MNase-ChIP, the buffer of the MNase reaction mixture was adjusted to be compatible to FA-lysis buffer (50 mM HEPES-KOH, pH 7.5, 140 mM NaCl, 1 mM EDTA, 1% Triton X-100, 0.1% sodium deoxycholate, EDTA-free protease tablet). The following salts were added to the MNase reaction tube: 80 µL of 0.5 M HEPES-KOH, pH 7.5, 22.4 µL of 5 M NaCl pre-mixed with protease inhibitors. This was followed by the addition of detergents, 6.4 µL of 12.5% sodium deoxycholate and 80 µL of 10% Triton X-100 per 600 µL MNase reaction.

The protein-G dynabeads (ThermoFisher Scientific) were pre-incubated with the antibodies for one hour at 4°C on a rotor, 85 µL beads/reaction. The antibodies used were anti-H3 (Abcam ab1791):12 µL per reaction; anti-H3K36me3 (Abcam ab9050): 6 µL per reaction; anti-H3K18ac (abcam ab1191): 7 µL per reaction; H4ac (Merck Millipore 06-598): 10 µL per reaction. The beads were washed in FA-lysis buffer twice, followed by incubation with the MNase-treated chromatin for 4 hours at 4°C on a rotor. The beads were sequentially washed with 1 mL of FA-Lysis buffer, 1 mL FA500-lysis Buffer (FA-Lysis Buffer + 500 mM NaCl), 1 mL of Buffer III (10 mM Tris-HCl, pH 8.0, 1 mM EDTA, 250 mM LiCl, 0.5% NP-40, 0.05% sodium deoxycholate), 1 mL of Tris-EDTA pH 8.0. For elution, the beads were incubated in 150 µL of elution buffer at 65 °C for 15 minutes.

The crosslinking was reversed by incubation of the eluate at 65°C overnight followed by the addition of 150 µL of TE (10 mM Tris-HCl, pH 8.0, 1 mM EDTA). The eluate was then treated with proteinase K (1 µg/µL final concentration) for 3 hours at 42°C. The DNA was purified using the NucleoSpin Gel and PCR clean-up kit (Macherey-Nagel) using the SDS protocol provided in the manual. The DNA concentration was measured using Qubit dsDNA HS assay kit (Invitrogen) and the libraries were prepared using NEBnext Ultra DNA library prep kit for Illumina (NEB). Finally, samples were paired-end sequenced at the iGE3 genomics platform of the University of Geneva.

ChEC-seq

The experiment was performed as described in (Zentner et al., 2015) after some modifications. The yeast strains were cultured the day before in YEPD medium. They were diluted to OD_{600}=0.2 in YEPD medium in the morning. The 60 min rapamycin treatment was performed at OD_{600}=0.4.

For each condition, 50 mL cell cultures were harvested at room temperature. The cells were washed twice in 1 mL Buffer A (15 mM Tris-HCl pH 7.5, 80 mM KCl, 0.1 mM EGTA, 0.2 mM spermine, 0.5 mM spermidine and protease inhibitor tablet (Sigma-Aldrich). Cells were resuspended in 594 µL of buffer A and 6 µL of 10% digitonin (0.1% final concentration) were added to permeabilize the cells during 5min at 30°C. $CaCl_2$ was added (final concentration 5 mM) to activate the MNase cleavage. 200 µL were collected at 30s for *SPT15-MNase* or 20s for *STH1-MNase* and were immediately mixed with 200 µL of 2X Stop solution (400 mM NaCl, 20 mM EDTA, 4 mM EGTA, 1% SDS).

The cells were treated with Proteinase K (0.4 µg/µL final concentration) and incubated at 55°C for 30 minutes. The DNA was extracted using phenol:chloroform:isoamyl extraction, and precipitated by adding 30 µg glycogen, 500 µL of 100% ethanol and incubated at -20°C for one hour. RNAse treatment was performed by adding 34.5 µL of Tris, pH 8.0 and 10 µg of RNAse per reaction.

For size selection of DNA fragments, 75 µL of solid phase reversible immobilization beads (SPRI, AmpureXP Beckman Coulter) were added in 25 µL of RNAse treated DNA and the reaction was mixed by pipetting up and down 10 times. The beads were incubated at room temperature for 5 minutes. The tubes were placed in the magnetic rack and supernatant was transferred to the new tube containing 10 mM Tris and 0.2 M NaCl for each reaction. The DNA was extracted with phenol:chloroform:isoamyl solution and precipitated with 100% ethanol.

The pellets were washed with 70% ethanol and resuspended in 29 µL of Tris, pH 8.0. DNA concentration was measured using Qubit dsDNA HS assay kit (Invitrogen) using 4 µL sample. The remaining 25 µL were used to prepare sequencing libraries using NEBnext Ultra DNA library prep kit for Illumina (NEB). The samples were sequenced in the paired-end mode at the iGE3 genomics sequencing platform in Geneva.

ATAC-seq

The experiment was performed after combining the protocols from (Buenrostro et al., 2013; Buenrostro et al., 2015; Schep et al., 2015) and (Au - Grbesa et al., 2017). The yeast strains were inoculated the day before in YEPD. Cultures were diluted to OD_{600}=0.2 and allowed to reach OD_{600}=0.4. Half of the culture was then treated with Rapamycin for 1h at 30°C.

1 mL of the cell culture was harvested from all conditions and strains. Cells were washed twice in 1 mL sorbitol buffer (1.4 M Sorbitol, 40 mM HEPES-KOH, pH 7.5, 0.5 mM $MgCl_2$) and were resuspended in 190 µL of sorbitol buffer and 10 µL of 10 mg/mL Zymolyase (20T Zymolyase, AMSBIO) and incubated at 30°C shaking at 200 rpm for 30 minutes. The cells were washed twice in sorbitol buffer and the incubated in 95 µL of 1x TD buffer and 5 µL of the TD enzyme (Illumina). The reaction was incubated at 37 °C at 500 rpm for 30 minutes. DNA was then extracted with 3x SPRI beads (AmpureXP Beckman Coulter) and eluted in 28 µL 10 mM Tris-HCl, pH 8.0.

Initial PCR amplification was performed with 4 µL of transposed DNA to check the transpositions and cycles required. Final amplification was performed with NEBNext High-Fidelity 2x PCR Master Mix (NEB) using Nextera Primers (Illumina). 12 cycles were performed.

The size selection was performed by sequential SPRI beads precipitation. First, the DNA was mixed by pipetting in 0.5x beads followed by incubation for 5 minutes at room temperature. The supernatant was used for the next DNA precipitation with 2.5x SPRI beads. The supernatant was discarded and the beads were washed with 70% ethanol twice before the DNA was extracted using 28 µL of 10 mM Tris-HCl, pH 8.0. The DNA concentration was measured and the samples were paired-end sequenced at the iGE3 genomics platform of the University of Geneva.

ChIP-qPCR

The experiments were performed as described in (Kuras and Struhl, 1999; Strahl-Bolsinger et al., 1997) after some modifications. For both *S. cerevisiae* and *S. pombe* (used here for spike-in), the cultures were grown to exponential phase until OD_{600}=0.5, after which they were treated with Rapamycin for different time points. Cells were fixed and chromatin was extracted as in the MNase(-ChIP)-seq section with the exception of the breaking step performed in FA-lysis buffer (50 mM HEPES-KOH, pH 7.5, 140 mM NaCl, 1 mM EDTA, 1% Triton X-100, 0.1% sodium deoxycholate, EDTA-free protease tablet). Chromatin was sheared to 300 bp fragments through sonication (Bioruptor, Diagenode).

2/3rd *S. cerevisiae* chromatin was mixed with 1/3rd of *S. pombe* chromatin. The ChIP was performed with the mixture using on average 200 µL of the ChIP chromatin at a concentration of 20 µg/mL. The rest of the experiment was performed as in the MNase(-ChIP)-seq section. After elution and clean-up, DNA fragments were amplified with the different oligos of Suppl. Table 2 using the SYBR Green PCR Master Mix (Applied Biosystems) and a Real-Time PCR machine (Bio-Rad).

List of genes, TBS and -1/+1 nucleosomes

The list of gene coordinates from TSS to poly-A was kindly provided by the Mellor Lab (Fischl et al., 2017). Among them were picked the ones considered as "Verified" genes in the Saccharomyces Genome Database (SGD) giving a complete list of 4,775 coding genes. For the TBS coordinates, our list was crossed with the data from the Pugh lab (Rhee and Pugh, 2012). -1/+1 coordinates were extracted from DANPOS2 analysis with default settings (Chen et al., 2013) from our bigWig profile of H3K18ac in -Rap.

RNA-seq analysis

Single-end reads were aligned to sacCer3 genome assembly using Bowtie2 (Langmead and Salzberg, 2012; Langmead et al., 2009) with options '-k 20 --end-to-end --sensitive -X 800'. PCR duplicates were removed from the analysis. BigWig coverage files were generated using Bam2wig function. Differential expression analysis was performed using the R/Bioconductor package DEseq on mRNA annotations Ensembl (Saccharomyces_cerevisiae.EF4.65.gtf). Antisense transcripts with a fold-change of at least 2 and multiple testing adjusted p-value lower than 0.05 were considered differentially expressed.

Among them, AMRG were defined as the genes showing a <0.8 fold-change with an adjusted p-value < 0.05.

MNase(-ChIP)-seq mapping

Paired-end reads were aligned to sacCer3 genome assembly using Bowtie2 (Langmead and Salzberg, 2012; Langmead et al., 2009) with options '-k 20 --end-to-end --sensitive -X 800'. PCR duplicates were removed from the analysis. Then, deepTools 2.0 (Ramirez et al., 2016) was used through the bamCoverage function with size selection of fragments (120-200bp to visualize only proper nucleosomes and not "fragile nucleosomes" (Brahma and Henikoff, 2019; Kubik et al., 2015)) and counting of only the 3 bp at the center of fragments.

ChEC-seq and ATAC-seq mapping

Paired-end reads were aligned to sacCer3 genome assembly using Bowtie2 (Langmead and Salzberg, 2012; Langmead et al., 2009) with default options from the Galaxy server (Afgan et al., 2018). PCR duplicates were removed from the analysis. DeepTools 2.0 (Ramirez et al., 2016) was then used through the bamCoverage function with size selection of fragments (0-120bp, 0-120bp and 120-200bp for TBP-ChEC, ATAC-seq and Sth1-ChEC respectively) and counting of only the 3bp at the center of fragments.

Metagene analyses

Bigwig files of independent duplicates generated *via* mapping were then averaged in deepTools 2.0 using the bigWigCompare command (however, results of each duplicate are shown in Suppl. Figures). Metagene plots were produced using computeMatrix followed by plotProfile commands. +Rap/-Rap fold-changes around TBS or -1/+1 nucleosomes were calculated adding no pseudo-count for ATAC-seq, TBP-ChEC and Sth1-ChEC, a pseudo-count of 1 for RNAPII PAR CLIP and a pseudo-count of 0.01 for MNase-seq, H3K36me3, H3K18ac and H4ac marks.

Figures 6A, B, C and D were normalized as follows: the mean of +Rap/-Rap fold-change was normalized to 1 in both *WT* and *rpd3Δ* strains giving a normalization factor for each strain. These normalization factors were then applied to the different classes to correct the raw fold-changes.

Statistical analyses

All plots and statistical analyses of this work were performed using Prism 8.0 (Graphpad). All tests are nonpaired tests (with the exception of Figures 6A-D based on paired tests). *t*-tests or Mann–Whitney *U* tests were used according to the normality of the data analyzed, which was calculated using a d'Agostino-Pearson omnibus normality test. * if p-value < 0.05, **< 0.01, *** < 0.001, ****<0.0001.

Data and Software availability

The accession number for the data reported in this study is GEO: GSE130946. RNAPII PAR CLIP data in Nrd1-AA were retrieved from (Schaughency et al., 2014). Nucleosome profiles in the Sth1-AA strain were generated by (Kubik et al., 2018).

Key Resources Table

REAGENT or RESOURCE	**SOURCE**	**IDENTIFIER**
Antibodies		
Anti-H3	Abcam	ab1791
Anti-H3K18ac	Abcam	ab1191
Anti-H4ac	Merck Millipore	06-598
Anti-H3K36me3	Abcam	ab9050
Critical Commercial Assays		
TD Buffer	Illumina	#15027866
TDE1 enzyme	Illumina	#15027865
Nextera Index Kit	Illumina	#FC-121-1011
NEBnext Ultra II DNA Library preparation kit	NEB	E7645
Chemicals, Peptides and Recombinant Proteins		

Micrococcal Nuclease	Thermo Scientific	88216
Deposited Data		
Raw and analyzed data	This paper	GEO: GSE130946
RNAPII PAR-CLIP in Nrd1-AA	(Schaughency et al., 2014)	GEO: GSE56435
MNase-seq in Sth1-AA	(Kubik et al., 2018)	GEO: GSE98260
Software and Algorithms		
Bowtie2	(Langmead and Salzberg, 2012)	http://bowtie-bio.sourceforge.net/bowtie2/index.shtml
deepTools	(Ramirez et al., 2016)	https://deeptools.readthedocs.io/en/develop/index.html
Danpos2	(Chen et al., 2013)	https://sites.google.com/site/danposdoc/
Galaxy	(Afgan et al., 2018)	https://usegalaxy.org/
Prism 8	GraphPad	N/A
Experimental Models: Organisms/Strains		
S. cerevisiae AA (FSY4885)	(Haruki et al., 2008)	*MAT α, tor1-1, fpr1Δ::NAT, RPL13A-2×FKBP12::TRP1*
S. cerevisiae Nrd1-AA (FSY5065)	(Castelnuovo et al., 2014)	*MAT α, tor1-1, fpr1Δ::NAT, RPL13A-2×FKBP12::TRP1, NRD1-FRB::KanMX6*
S. cerevisiae Nrd1-AA *rpd3Δ* (FSY7015)	This study	*MAT α, tor1-1, fpr1::NAT, RPL13A-2×FKBP12::TRP1, NRD1-FRB::KanMX6, rpd3Δ::HIS3*
S. cerevisiae Nrd1-AA TBP-MNase (FSY8162)	This study	*MAT α, tor1-1, fpr1::NAT, RPL13A-2×FKBP12::TRP1, NRD1-FRB::KanMX6, TBP-MNase::HPHMX6*

S. cerevisiae Nrd1-AA *rpd3Δ* TBP-MNase (FSY8164)	This study	*MAT α, tor1-1, fpr1::NAT, RPL13A-2×FKBP12::TRP1, NRD1-FRB::KanMX6, rpd3Δ::HIS3, TBP-MNase::HPHMX6*
S. cerevisiae Nrd1-AA STH1-MNase (FSY8254)	This study	*MAT α, tor1-1, fpr1::NAT, RPL13A-2×FKBP12::TRP1, NRD1-FRB::KanMX6, STH1-MNase::HPHMX6*
S. cerevisiae Nrd1-AA *rpd3Δ* STH1-MNase (FSY8255)	This study	*MAT α, tor1-1, fpr1::NAT, RPL13A-2×FKBP12::TRP1, NRD1-FRB::KanMX6, rpd3Δ::HIS3, STH1-MNase::HPHMX6*
Oligonucleotides		

See Suppl. Table 2

Supplemental Information

Supplementary Figures 1-7

Supplementary Table 1 - Strains and growth of the strains used in this study

Supplementary Table 2- Oligonucleotides used in this study

Supplementary Figure Legends

Supplementary Figure 1. Related to Figure 1

(A) Box-plots showing the +Rap/-Rap fold-change for the RNA-seq in the Nrd1-AA strain. Fold-change is calculated based on the coverage in the -100bp to Transcription Start Site (TSS) region for antisense and over the whole transcript for the sense.
(B) Metagene analysis and heatmap depicting the TBP-ChEC profile in the Nrd1-AA in the absence of Rap. Results are centered on the TATA-Binding Site (TBS).
(C) Box-plots of the two independent replicates of TBP-ChEC fold-change related to Figure 1D. The fold-change is measured over a 100bp region centered on the TBS.

Supplementary Figure 2. Related to Figure 2

(A) Box-plots of the two independent replicates of MNase-seq fold-change related to Figure 2C. The fold-change is measured over a 100bp region centered on the TBS.
(B) Metagene of MNase-seq in Nrd1-AA treated or not for 1h with Rap. Midpoint of 120-200bp paired-end fragments are represented. Results are centered on the +1 nucleosome.
(C) ChIP of H3 at gene promoters of AMRG, NRG and Other genes. ChIPs were performed at 0, 30, 60, 90 and 120min after rapamycin addition. Immunoprecipitated promoter NDRs were normalized to immunoprecipitated *SPT15* ORF after qPCR amplification. Primers are designed to target promoter NDRs. The fold-change was artificially set to 1 for each gene in the -Rap condition. Error bars represent the Standard Error of the Mean (SEM) for a set of 3 independent experiments.

Supplementary Figure 3. Related to Figure 3

(A) Metagene plot of H3K36me3 MNase-ChIP-seq related to Figure 3A and centered on the +1 nucleosome. Midpoint of 120-200bp fragments are represented.
(B) Box-plots of the fold-change related to Figure 3B for the two independent replicates of H3K36me3 MNase-ChIP-seq. The fold-change is measured over a 100bp region centered on the TBS.

Supplementary Figure 4. Related to Figure 4

(A) Metagene plot of H3K18ac MNase-ChIP-seq related to Figure 4A and centered on the +1 nucleosome. Midpoints of 120-200bp fragments are represented.
(B) Box-plots of the fold-change related to Figure 4B for the two independent replicates of H3K18ac MNase-ChIP-seq. The fold-change is measured over a 20bp region centered on the -1 nucleosome.
(C) Metagene profiles of H4ac MNase-ChIP-seq levels centered on TBSs and -1 nucleosome obtained in an Nrd1-AA strain treated or not for 1h with Rapamycin. The centers of 120-200bp paired-end fragments are represented here. The grey boxes represent the 100bp and 20bp areas centered on the TBS and -1 nucleosome respectively.
(D) Box-plots indicating the +Rap/-Rap fold-change in H3K18ac levels in the 100bp TBS- and 20bp -1/+1-centered areas.

Supplementary Figure 5. Related to Figure 5

(A) Metagene plot of Sth1-ChEC centered on the +1 nucleosome. Midpoint of 120-200bp fragments are represented.
(B) Box-plots of the +Rap/-Rap fold-change related to Figure 5B for the two independent replicates of Sth1-ChEC. The fold-change is measured over a 20bp region centered on the -1 nucleosome.

Supplementary Figure 6. Related to Figure 6

(A) ChIP of H3K18ac levels at the promoters of AMRG, NRG and Other genes. *S. pombe* chromatin was used as a spike-in control and mixed with *S. cerevisiae* chromatin before immunoprecipitation. *S. cerevisiae* results are normalized to *S. pombe ACT1* ORF. All results are expressed as fold-change with respect to -Rap which value was set to 1.
(B) RNA-seq of AMRG antisense in Nrd1-AA +Rap vs Nrd1-AA *rpd3Δ* +Rap. Results are depicted in rpkm. The +Rap condition was chosen to have an accurate measurement of antisense production. r indicates the Pearson correlation. Even in the absence of Rpd3, antisense RNAs are globally well produced at AMRGs and the rescue of AMRG sense expression (Figure 6) is not a consequence of a lack of antisense production.

Supplementary Figure 7. Related to Figure 7

(A) Box-plots of expression by RNA-seq according to the quintiles defined in **Figure 7**.

(B) Metagene analysis of H4ac levels around the -1 nucleosome according to the quintiles defined in **Figure 7**.

(C) Natural nascent antisense levels in promoters and natural nascent sense levels of AMRG as compared to the quintiles defined in **Figure 7**.

(D) Metagene plot of MNase-seq profile at steady state for the AMRG as compared with the high and low antisense quintiles defined in **Figure 7**. Results are centered on the TBS.

(E) Cartoon explaining the molecular basis of the weak changes in the antisense inducible system in a model in agreement with our measurement.

(F) Global correlation between nascent antisense transcription into promoters (-100bp to TSS area) and nascent sense transcription (100bp area upstream of the poly-A site). The correlation coefficient r corresponds to the Pearson correlation.

(G) Metagene plot of H3K36me3 and H3K18ac dyads profiles in the Low antisense quintile at steady state (-Rap).

Figure 1

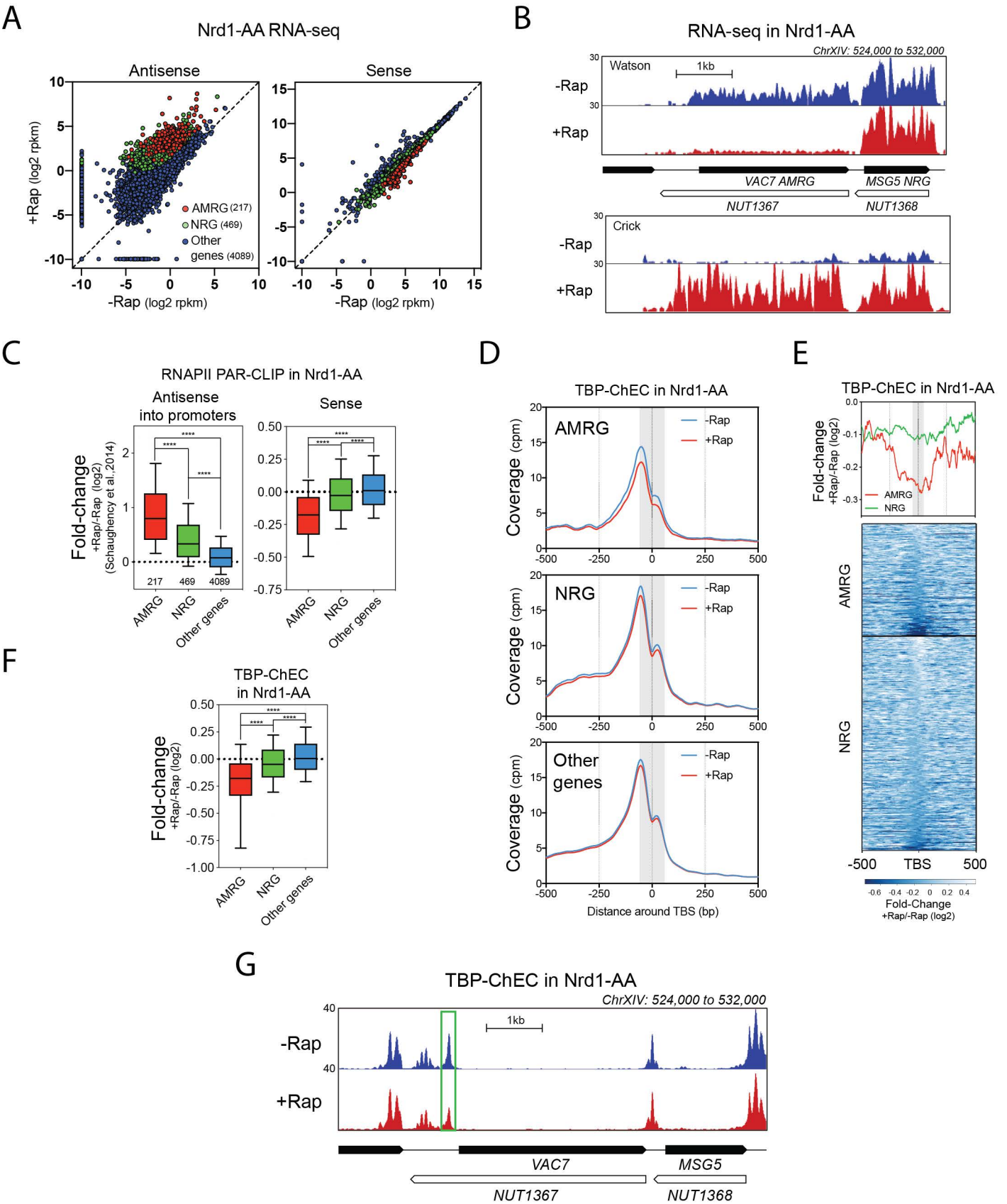

Figure 2

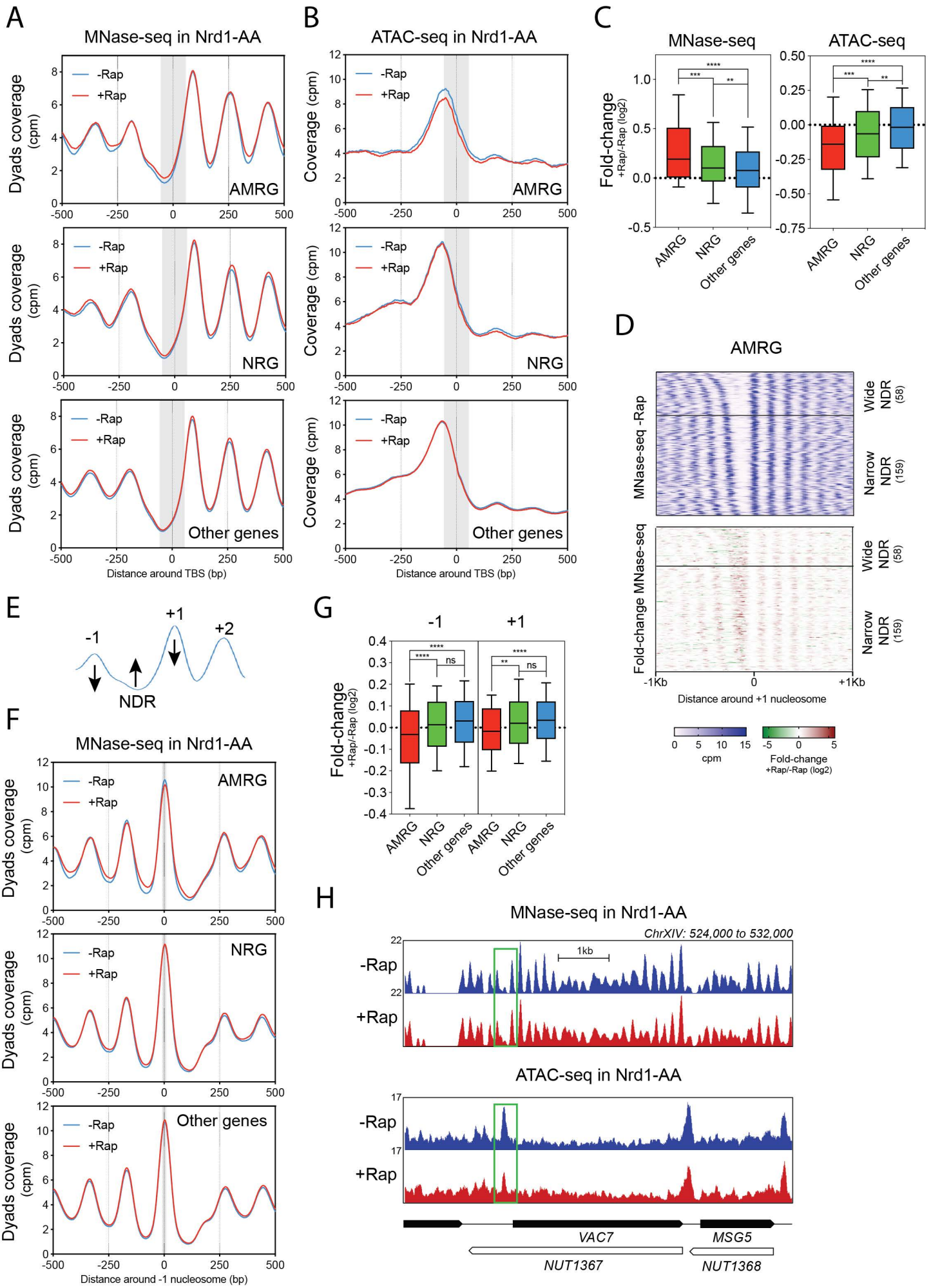

Figure 3

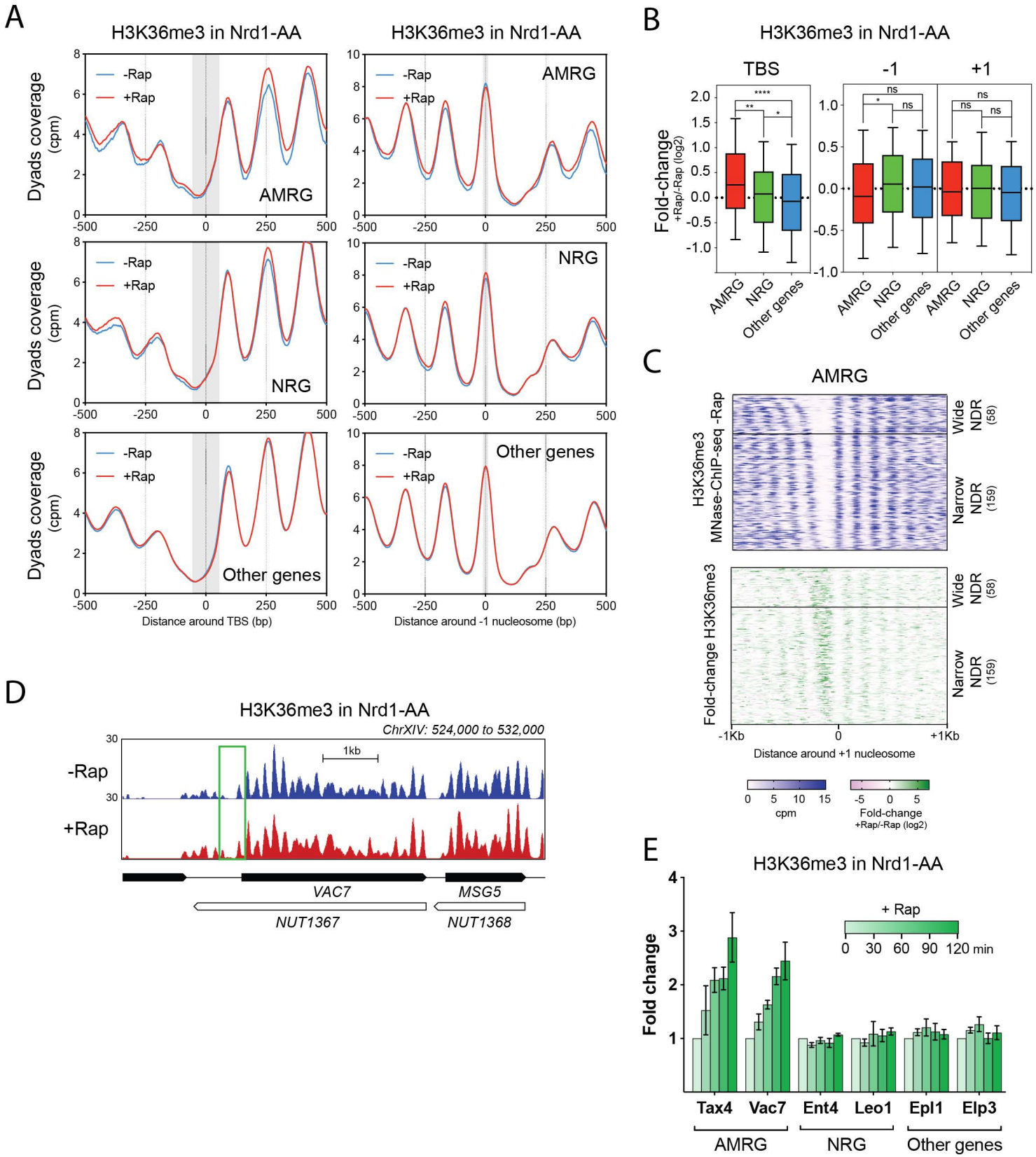

Figure 4

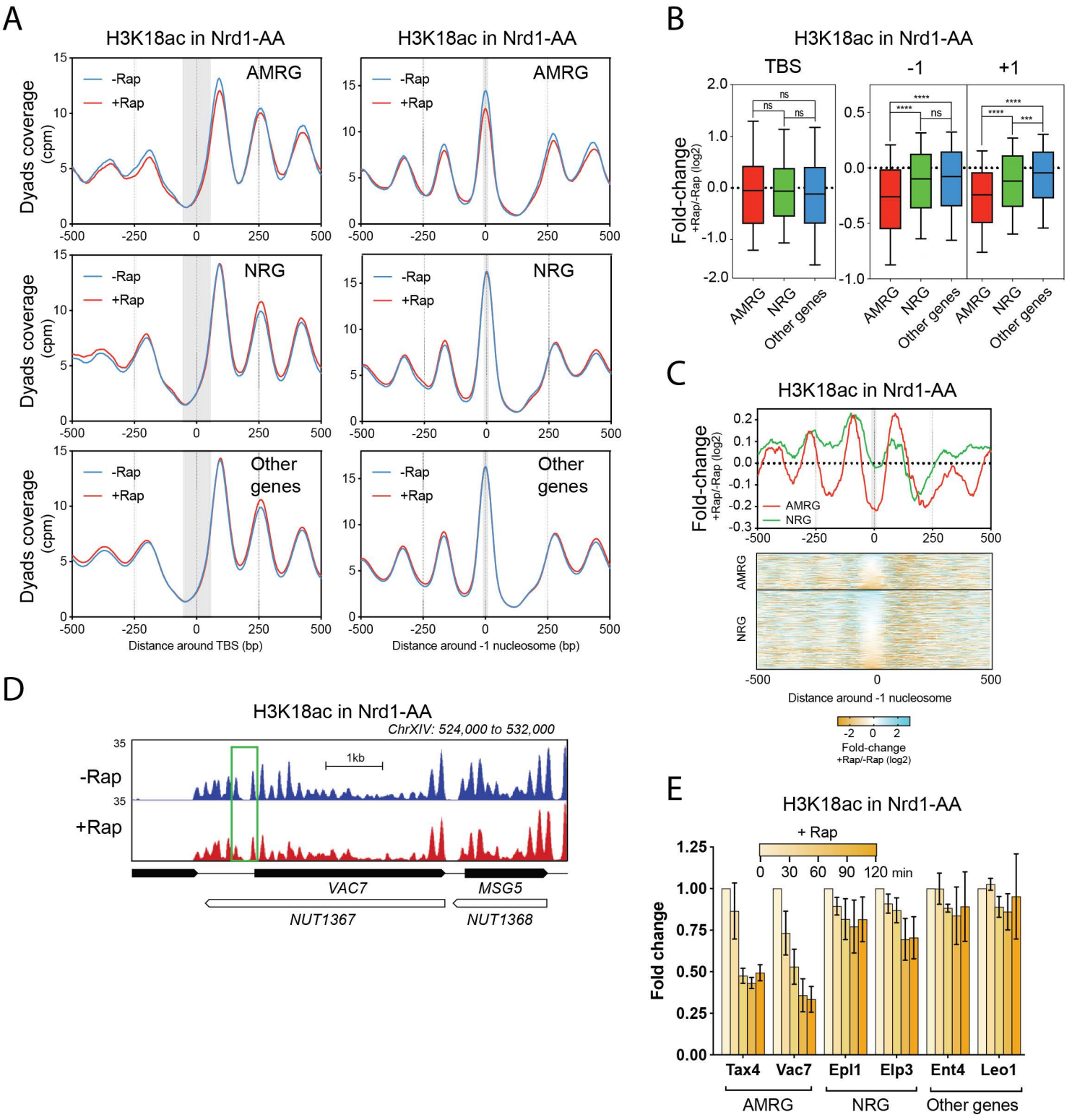

Figure 5

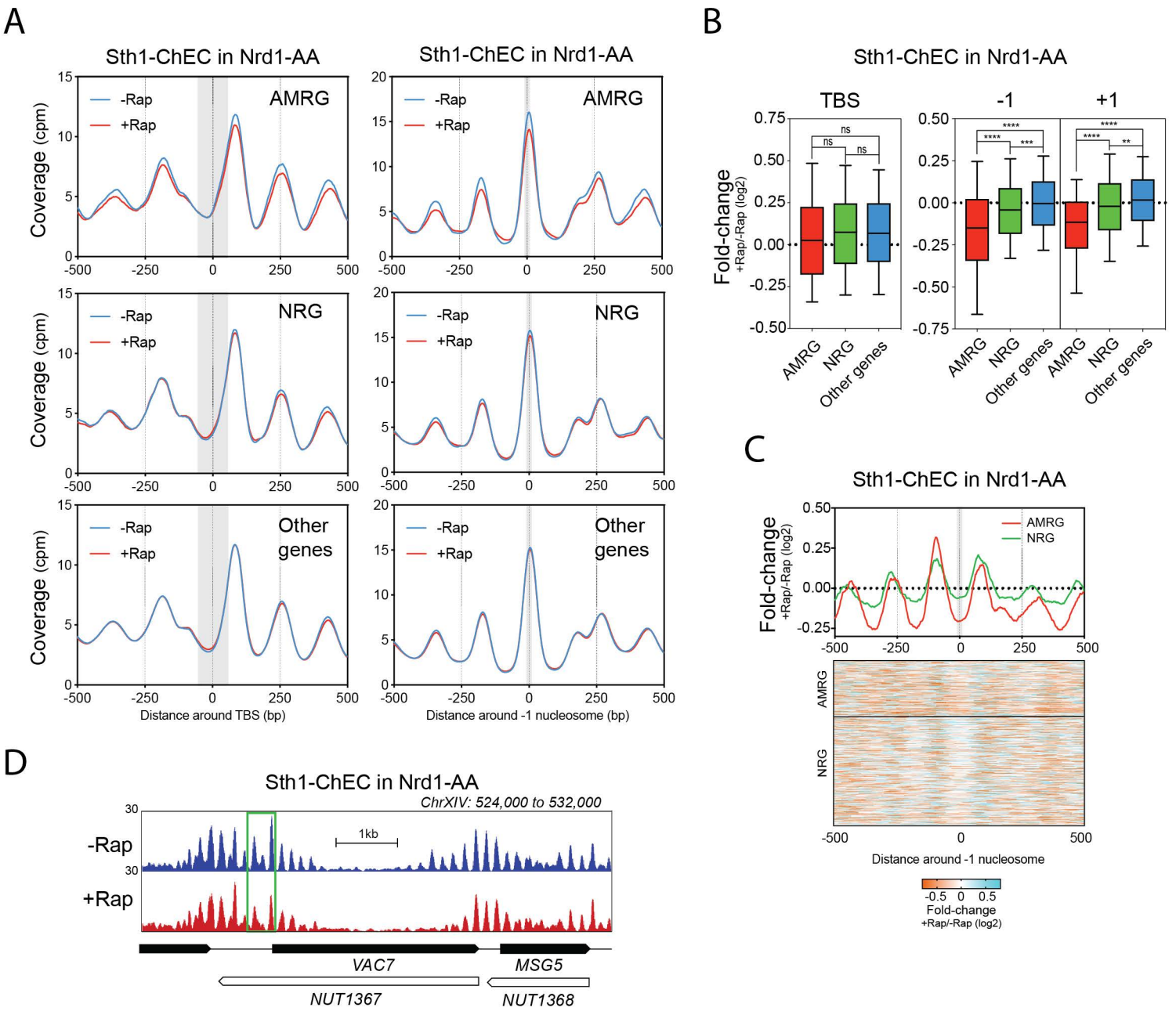

Figure 6

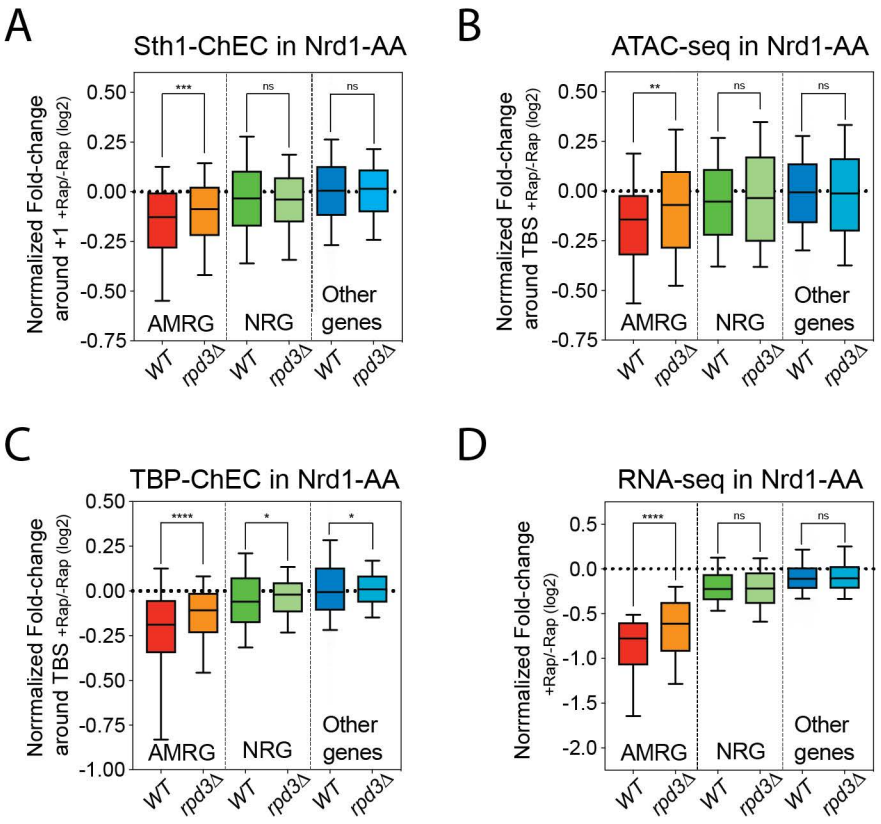

Figure 7

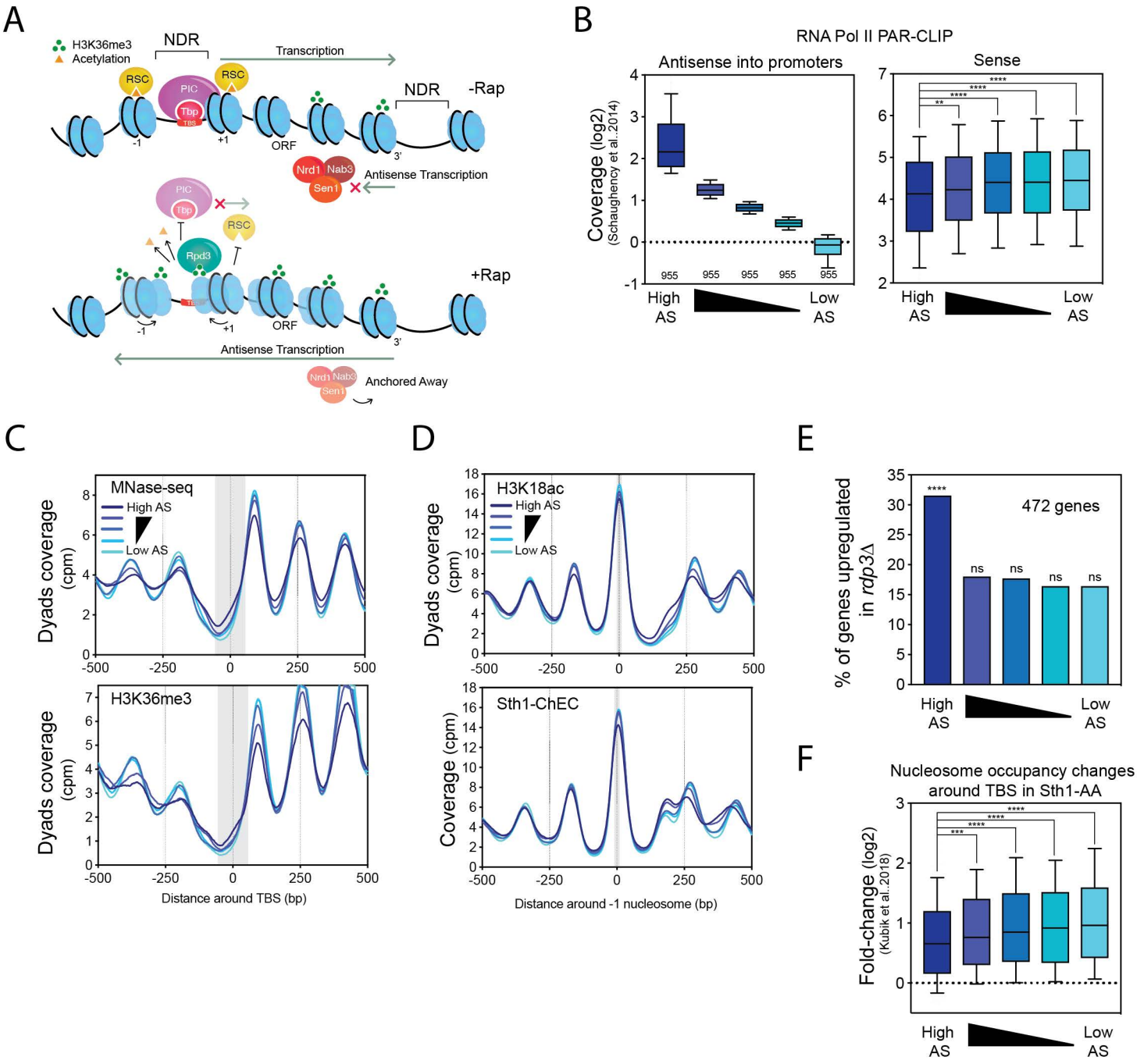

Suppl. Fig. 1

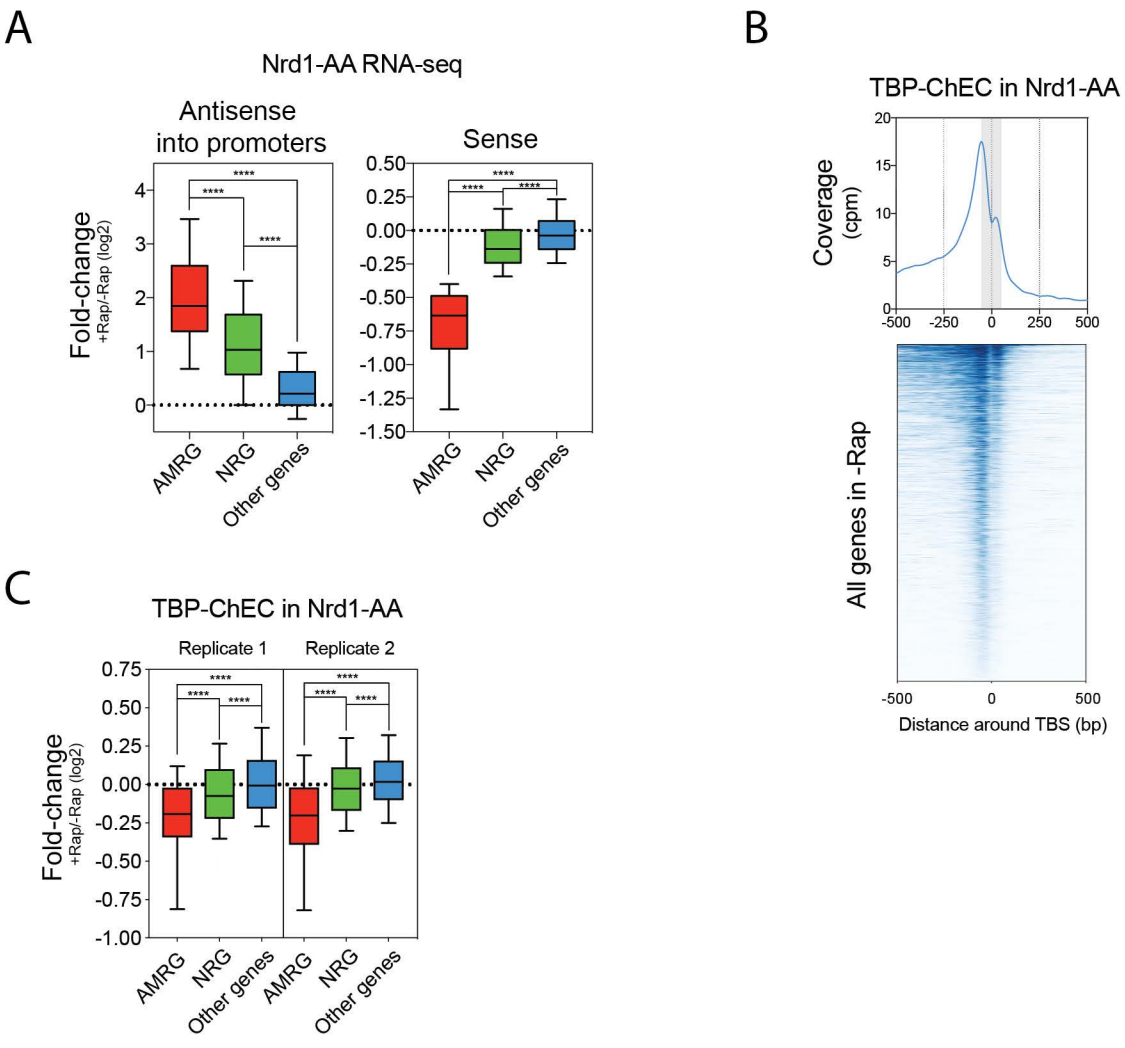

Suppl. Figure 2

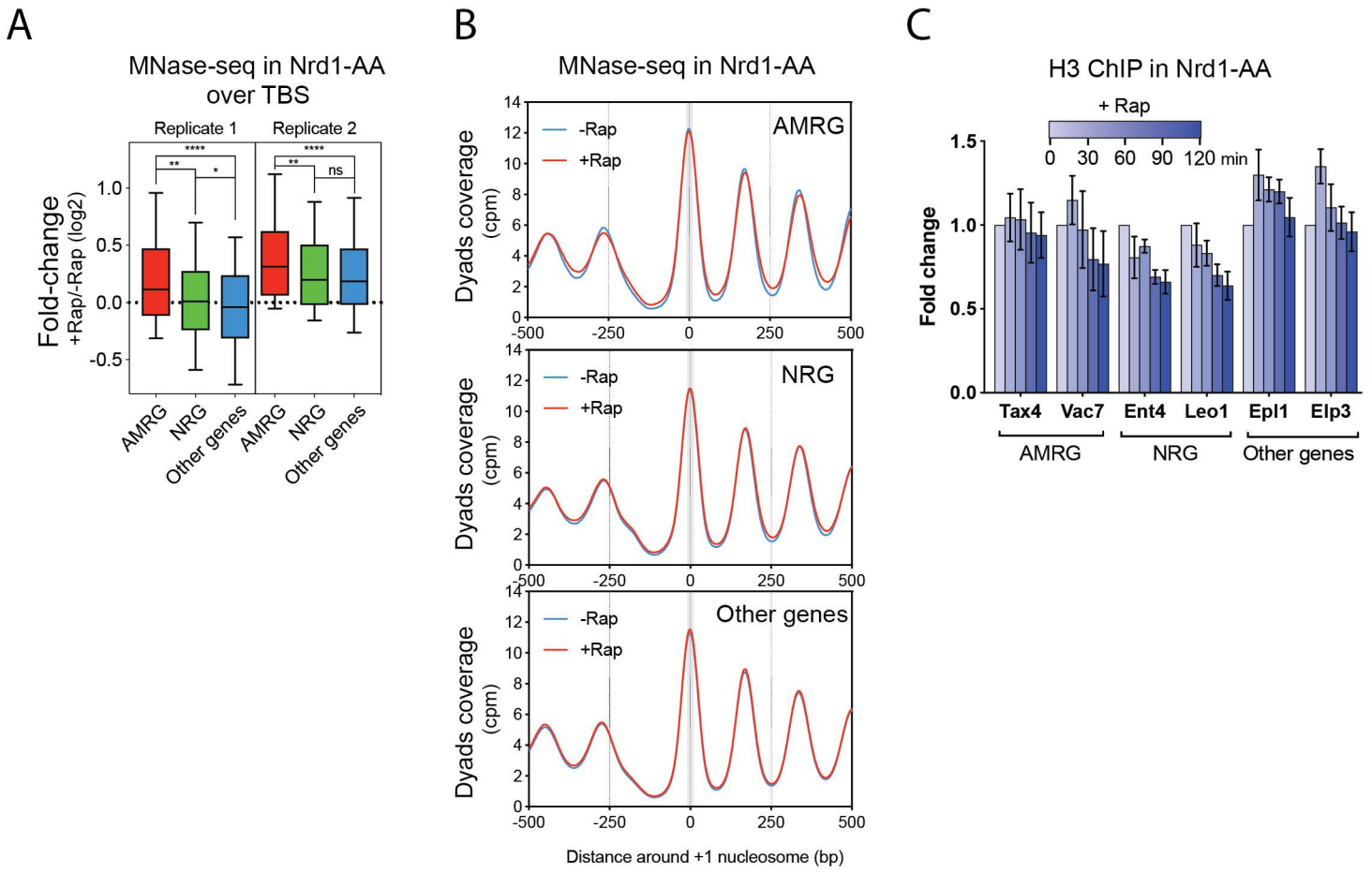

Suppl. Figure 3

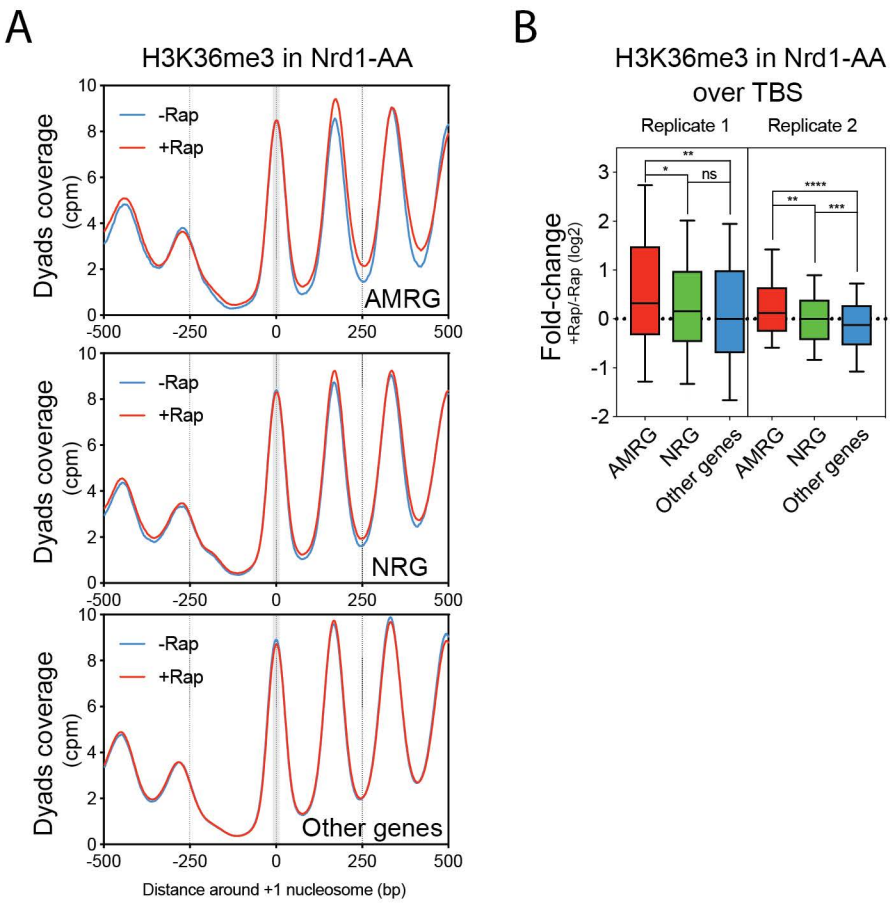

Suppl. Figure 4

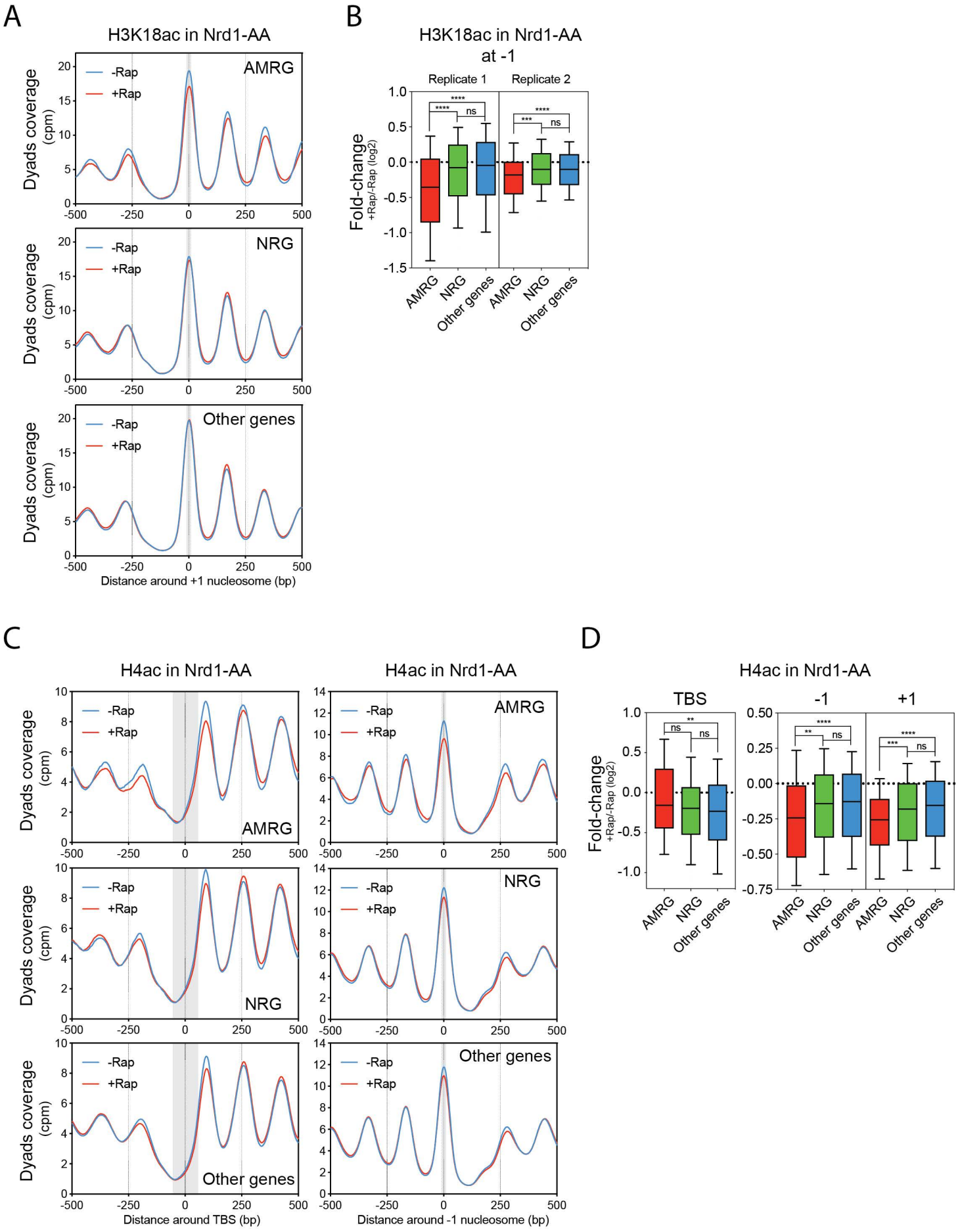

Suppl. Figure 5

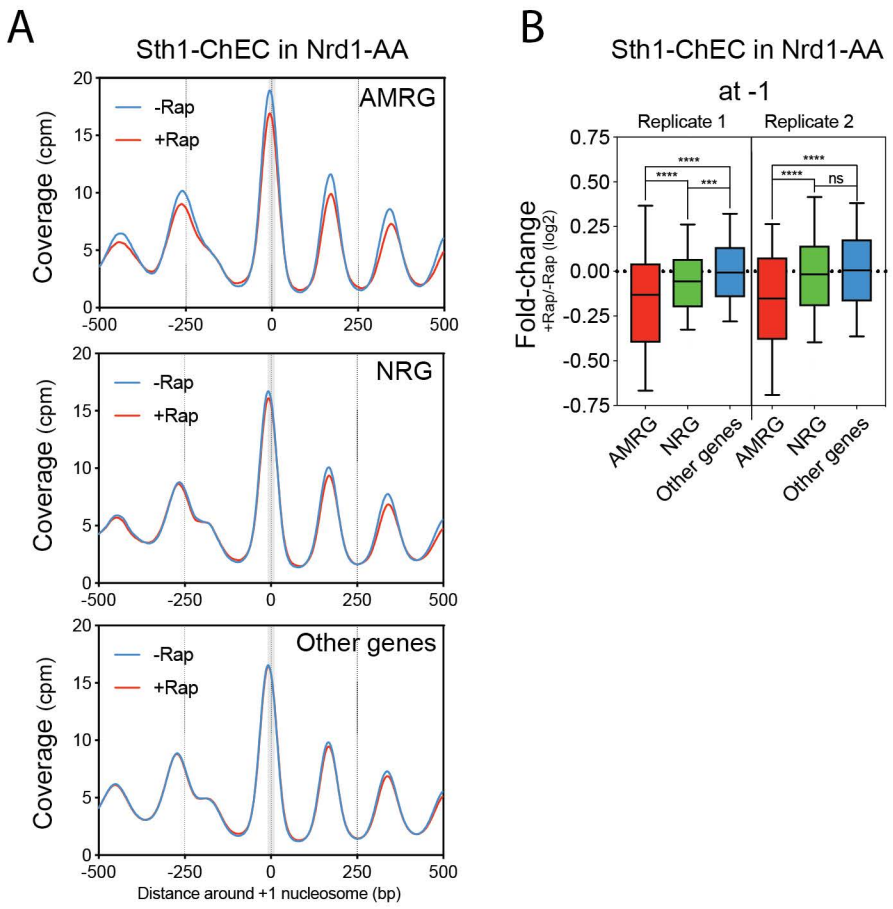

Suppl. Figure 6

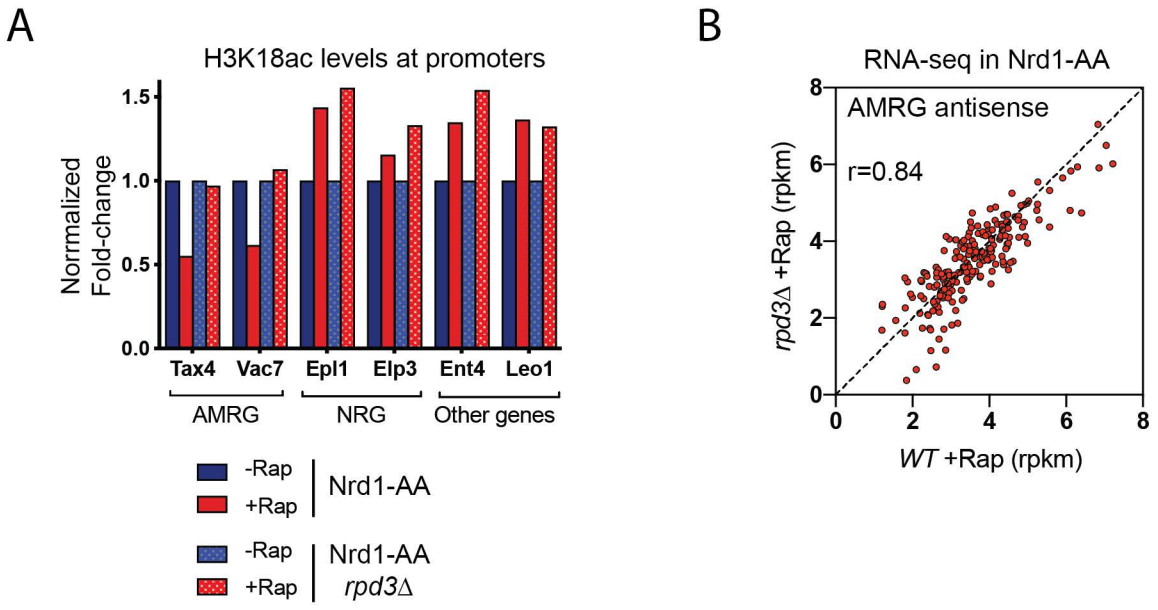

Suppl. Figure 7

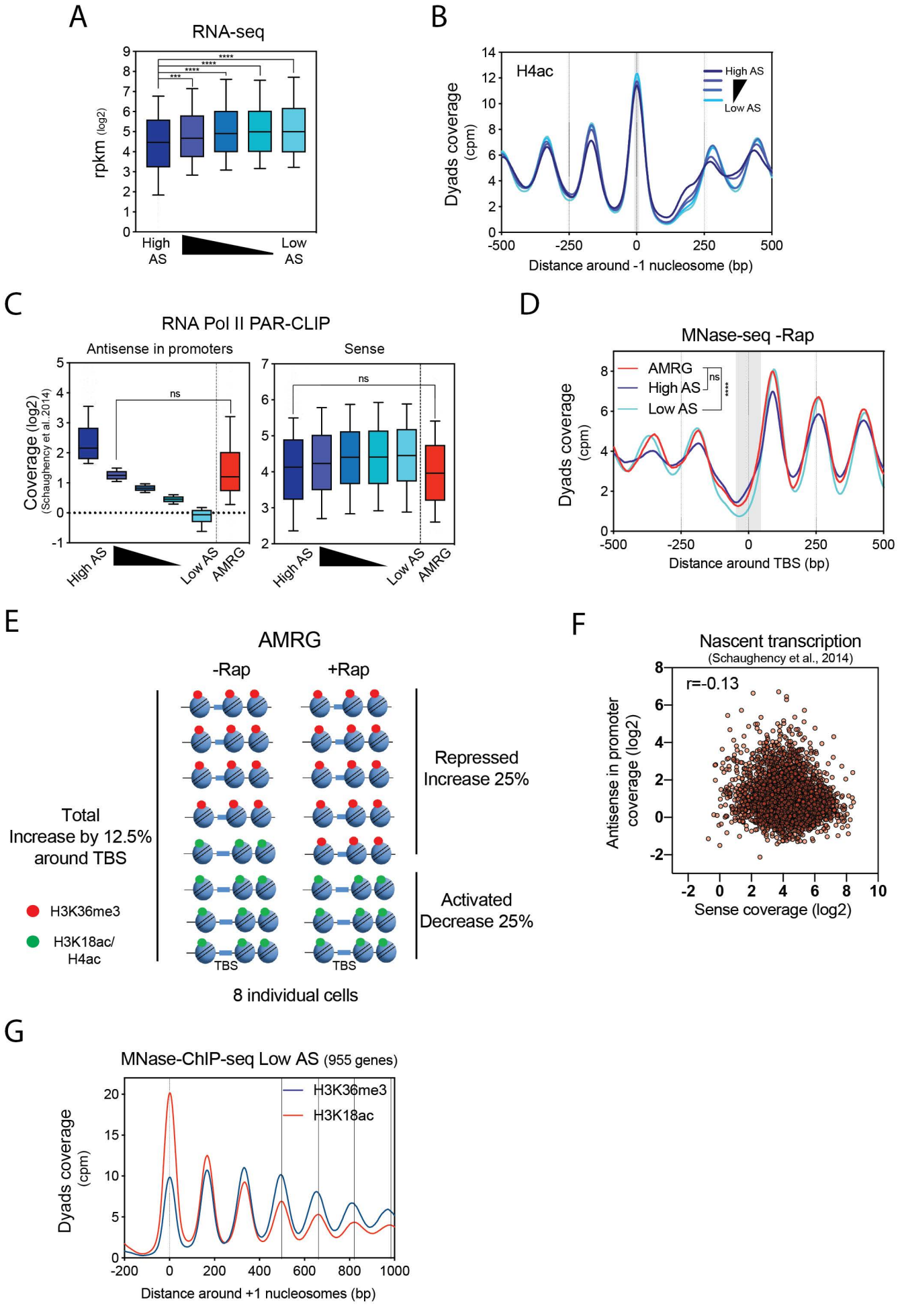

Suppl. Table 1

Experimental Models: Organisms/Strains		
S. cerevisiae AA (FSY4885)	(Haruki et al. 2008)	*MAT α, tor1-1, fpr1Δ::NAT, RPL13A-2×FKBP12::TRP1*
S. cerevisiae Nrd1-AA (FSY5065)	(Castelnuovo et al. 2014)	*MAT α, tor1-1, fpr1Δ::NAT, RPL13A-2×FKBP12::TRP1, NRD1-FRB::KanMX6*
S. cerevisiae Nrd1-AA *rpd3Δ* (FSY7015)	This study	*MAT α, tor1-1, fpr1::NAT, RPL13A-2×FKBP12::TRP1, NRD1-FRB::KanMX6, rpd3Δ::HIS3*
S. cerevisiae Nrd1-AA TBP-MNase (FSY8162)	This study	*MAT α, tor1-1, fpr1::NAT, RPL13A-2×FKBP12::TRP1, NRD1-FRB::KanMX6, TBP-MNase::HPHMX6*
S. cerevisiae Nrd1-AA *rpd3Δ* TBP-MNase (FSY8164)	This study	*MAT α, tor1-1, fpr1::NAT, RPL13A-2×FKBP12::TRP1, NRD1-FRB::KanMX6, rpd3Δ::HIS3, TBP-MNase::HPHMX6*
S. cerevisiae Nrd1-AA STH1-MNase (FSY8254)	This study	*MAT α, tor1-1, fpr1::NAT, RPL13A-2×FKBP12::TRP1, NRD1-FRB::KanMX6, STH1-MNase::HPHMX6*
S. cerevisiae Nrd1-AA *rpd3Δ* STH1-MNase (FSY8255)	This study	*MAT α, tor1-1, fpr1::NAT, RPL13A -2×FKBP12::TRP1, NRD1 -FRB::KanMX6, rpd3Δ::HIS3, STH1 -MNase::HPHMX6*

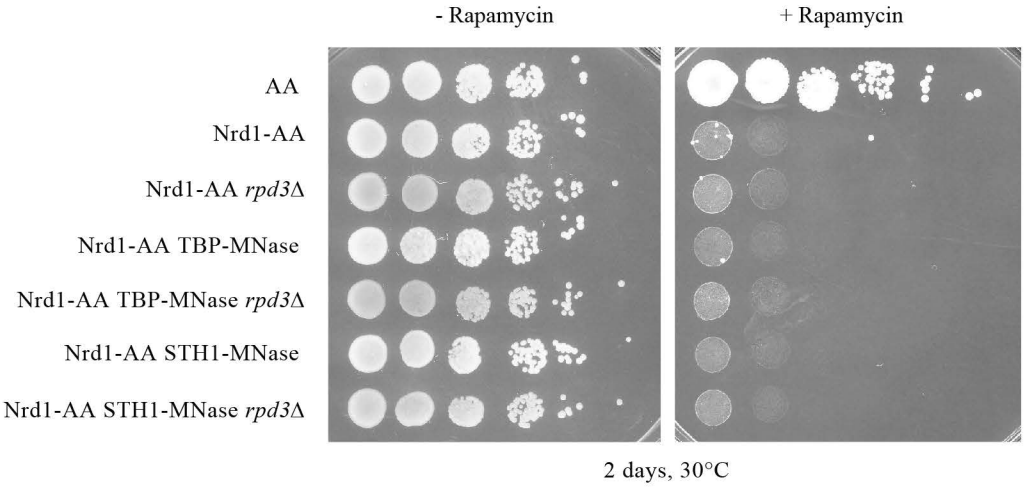

Suppl. Table 2

Oligos used		
TAX4	Forward	ATAGATGGCGCAAGGGAGTT
	Reverse	AAACGTCAGGGCGTGTATTC
VAC7	Forward	TGTAAGTCTTCCTGGCCACTC
	Reverse	GATCATTATGCAAAATCGAAGG
EPL1	Forward	GGAACGCGATGTGGTGTAAT
	Reverse	CACGATCCGACCACAAAAT
ELP3	Forward	CACTGGATAATTTGAGATGAGCTA
	Reverse	TTCAAAAGTCAATACTGCCACTG
LEO1	Forward	AAGCTTTGCCATATTCAATCG
	Reverse	GCTTTCGTATTCACTTCTATGAGC
ENT4	Forward	CGCTGACACGTTTGTACTTTC
	Reverse	CCTCAATTTTCGTTTTCTCATTC
ACT1 *S.pombe*	Forward	TCTTTTCCATATCATCCCAGTTG
	Reverse	CTCAAAGCAAGCGTGGTATTT
SPT15	Forward	TCGGGTTTGCTGCTAAATTC
	Reverse	ACACAATTTTCGGCTTCACC